Solvation and Friction in Supercritical Fluids: Simulation−Experiment Comparisons in Diphenyl Polyene/CO₂ Systems

N. Patel, R. Biswas, and M. Maroncelli*

Department of Chemistry, The Pennsylvania State University, University Park, Pennsylvania 16802

Received: March 11, 2002; In Final Form: May 2, 2002

Computer simulations of realistic models of the two solutes diphenylbutadiene ("DPB") and hydroxymethylstilbene ("HMS") in supercritical CO_2 (310 K, 0.25−2.0ρ_c) are used to explore the interplay between local density augmentation and friction in supercritical solvents. Good agreement is found between the extent of local density augmentation observed in these simulations and that deduced from experimental measurements of electronic spectral shifts (also reported here). To test the accuracy of the solvent model for treating solute friction, the viscosity and self-diffusion constants of the neat solvent were simulated and compared to experiment and good agreement was also found. The rotation times of these solutes are compared to results of prior experimental measurements made by Anderton and Kauffman (*J. Phys. Chem.* **1995**, *99*, 13 759). In the case of DPB, the simulated times are larger than experimental estimates by as much as 30% at higher densities ($\rho \approx 1.8\rho_c$). The origins of this disagreement are presently unknown. The density dependence of the simulated friction on both rotational and translational motions is curious in that it appears insensitive to the considerable density augmentation present in these systems. This insensitivity is shown to result from a cancellation of static and dynamic aspects of the friction, both of which are individually responsive to the excess density in the neighborhood of the solute.

I. Introduction

Supercritical fluids are finding increasing use as solvents both in a variety of practical applications[1−5] and in fundamental studies of solvation and solvent effects on chemical reactions.[1,6−8] In the latter realm, many studies have focused on understanding the density augmentation that occurs in the neighborhood of attractive solutes[8−12] and the impact that this augmentation has on simple processes such as solute diffusion,[13−19] vibrational relaxation,[20−25] and chemical reaction.[6,26−31] Computer simulations, primarily on simplified model systems, have been widely used in these efforts and have provided considerable insight into the nature of supercritical solvation and its influence on energetics and dynamics.

In the present paper, we report further molecular dynamics simulations, designed to explore friction in supercritical solvents. In particular, we focus on the rotational and translational friction felt by typical large solute molecules and examine how this friction varies with solvent density. Our work differs from past studies of this sort[13,32,15] in that we employ what we believe to be realistic models for both the solute and the solvent in order to make direct comparisons between the simulation results and experimental measures of both density augmentation and rotational friction.

The systems chosen for study are the two diphenylpolyenes, diphenylbutadiene "DPB" and hydroxymethylstilbene "HMS" (Scheme 1) in supercritical CO_2. These particular solutes are of interest for several reasons. First, some of the earliest measurements of rotational dynamics in supercritical solvents were made on these solutes in the pioneering study by Anderton and Kauffman.[19] Although a number of other measurements of solute rotation have appeared since that time[33,18] (including some from our own lab[17]), the systems studied by Anderton and Kauffman are still the most amenable to comparison with simulation. As will be discussed in more detail later, the size

SCHEME 1

"DPB"
(*trans,trans*-1,4-diphenyl-1,2-butadiene)

"HMS"
(*trans*-4-stilbenemethanol)
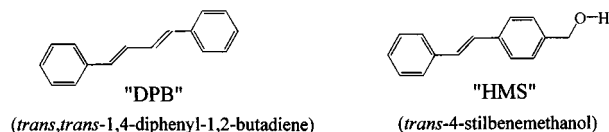
and shape of these two solutes are quite similar, the main difference being in their electrical characteristics and/or hydrogen bonding ability. Comparisons of the rotational dynamics of the two solutes can therefore be used to explore the importance of dielectric friction and solute−solvent association. For this reason, Kauffmann and co-workers have performed parallel studies of both solutes in a number of liquid solvents.[34,35] As a result of these and other studies,[36] the liquid-state rotational behavior of DPB and HMS are reasonably well established. Finally, we note that measurement of rotation times in these solutes is facilitated by the fact that both of them undergo rapid excited-state isomerizations in liquid solvents[37−41] and in supercritical fluids.[19,42−45] Although we do not address this reactive dynamics in the present work, understanding the rotational friction on these solutes will be useful in future studies of their isomerization reactions.

In the experimental study that forms the starting point of the present simulations, Anderton and Kauffman[19] used measurements of fluorescence lifetimes and steady-state emission anisotropies[46] to determine the rotation times of DPB and HMS in CO₂ at 35 °C, four degrees above the critical point. The rotation of both solutes was found to be rapid, varying between 3 and 11 ps over the accessible density range, 0.6−1.8ρ_c (ρ_c denotes the critical density). At lower densities the two solutes were found to rotate at roughly comparable rates, rates near to those calculated for isolated molecules. However, at densities above ∼1.5ρ_c, the rotation time of HMS increases markedly

Solvation and Friction in Supercritical Fluids

J. Phys. Chem. B, Vol. 106, No. 28, 2002 **7097**

compared to that of DPB. To interpret these findings, Anderton and Kauffman[19] analyzed their data using the quasi-hydrodynamic ("DKS") model of rotational friction due to Dote, Kivelson, and Schwartz.[47] They concluded that the local density in the vicinity of DPB differs little from that of the bulk fluid, whereas the local solvent density around HMS is ~40% greater than the bulk solvent density. By analogy to the pronounced differences in rotational times observed for HMS in liquid alkane versus alcohol solvents,[35] Kauffmann and co-workers attributed this difference in augmentation to the ability of HMS to hydrogen bond to CO_2.[42,43,19]

Part of our motivation for simulating these particular experimental systems stems from several aspects of the above results that, in hindsight, appear curious. First, given the ubiquity of density augmentation now known to exist in a wide range of solutes of comparable size and attractiveness to DPB,[10,8] its apparent absence in the DPB/CO_2 system is puzzling. Of course, the conclusion concerning DPB rests upon modeling the rotational dynamics using the DKS model. Although this model has proven successful in explaining the rotation of molecules such as DPB in some liquid solvents[34,48−50] it is far from universally applicable,[51] and it would not be surprising to see it yield inaccurate predictions at supercritical densities. In addition, as already discussed by Kauffman,[43,19] relating rotation times to solvent friction also depends sensitively on how the free rotor limit is treated, and rather different conclusions concerning the extent of density augmentation can be drawn from the same data depending on one's approach.[52] Given these uncertainties, simulations are valuable both for examining the extent of augmentation in these systems as well as for providing guidance on how to interpret rotation times in terms of solvent friction. Another curious feature of the experimental data is the fact that large differences in the rotation times of DPB and HMS were only observed at higher bulk densities. If these differences are in fact due to the presence of solute−solvent interactions in the HMS/CO_2 system, one might have anticipated that the greatest differences in solute−solvent association and thus rotation times would occur at low solvent densities, rather than at high densities where augmentation should be small. Simulations should be helpful in understanding the sorts of solute−solvent association present in these systems and thus in explaining this counter-intuitive observation. Finally, apart from these comparisons to experiment, the present simulations were undertaken in order to provide general insights into the nature of friction and its evolution with density in supercritical solvents.

The remainder of this paper is structured as follows: Section II describes the models used to represent the solvent and solutes, and discusses results of electronic structure calculations used to develop the solute models. The simulation methodology, as well as the experimental procedures for measuring electronic absorption spectra (used for determining local densities independent of rotation measurements) are detailed in section III. The results are then presented in four parts. Section IV.A describes general aspects of the solvation structure and energetics found in simulation. The simulations indicate significant and comparable density augmentation exists in both the DPB/CO_2 and the HMS/CO_2 systems. In section IV.B, we compare the augmentation found in simulation with that deduced from experimental measurements of spectral shifts. In this respect, the experiment and the simulation are in good if not perfect agreement, with the experiments apparently showing slightly greater augmentation than the spectral shifts. Because very few realistic simulation−experiment comparisons have been performed previously, we consider the level of agreement achieved

herein some detail. In section IV.C, we make similar comparisons concerning dynamics, beginning with the dynamics of the CO_2 solvent itself, and then between simulated and observed rotation times of DPB and HMS. Although the CO_2 model[53] we employ provides reasonably accurate predictions for several dynamical properties of the pure solvent, the agreement between simulation and experiment is less satisfying when it comes to solute rotation. The rotation times simulated for DPB at higher densities are ~30% larger than the experimental estimates. The simulations also fail to show the large difference in the rotation times of DPB and HMS displayed by the experimental data. Possible explanations for the disagreement are considered, but no definitive conclusions can be reached at this point. Finally, in section IV.D, we use the simulation results to explore the density dependence of the friction on solute rotation and translation in more detail. The net friction on both types of motion exhibits an apparent lack of sensitivity to the substantial density augmentation present in these systems. Further analysis shows how this unexpected behavior comes about via opposing effects of local density on the static and dynamic components of the friction.

II. Simulation Models

Molecules were modeled as rigid collections of atomic sites interacting through site−site Lennard−Jones plus coulomb terms

$$u_{ij} = 4\epsilon_{ij}\left\{\left(\frac{\sigma_{ij}}{r_{ij}}\right)^{12} - \left(\frac{\sigma_{ij}}{r_{ij}}\right)^{6}\right\} + \frac{q_i q_j}{r_{ij}}$$
$$\text{with } \sigma_{ij} = \frac{1}{2}(\sigma_{ii} + \sigma_{jj}) \text{ and } \epsilon_{ij} = \sqrt{\epsilon_{ii}\epsilon_{jj}} \quad (1)$$

For the CO_2 solvent, the site parameters ϵ_i, σ_i, and q_i, as well as the geometry, were taken from the "EMP2" potential of Harris and Yung,[53] which was constructed to reproduce the coexistence curve of the real fluid. (We show later that this model also does a good job of reproducing some dynamical features of CO_2 relevant in the present work.) The Lennard−Jones parameters of the solutes were taken from the OPLS parametrization of Jorgensen and co-workers.[54] A summary of all of the potential parameters as well as the solute geometries used in these simulations are provided in Supporting Information, Table 1.

Solute geometries were derived from ground-state electronic structure calculations.[55,56] Geometry optimizations at the AM1 and RHF/6-31G(d,p) levels showed that the planar ("C_{2v}") structures of both molecules were at slightly higher energy than structures in which the phenyl rings rotate out of the plane formed by the double bond(s). Minimum energies were found at twist angles (labeled "χ" in Figure 1) of roughly 20° in both solutes. However, the preference for these nonplanar geometries is calculated to be quite small, <1 kJ/mol in all cases. Such shallow torsional wells suggest that the location of these minima is probably of little consequence because the amplitude of torsional motion should be large, on the order of ±40° near room temperature.[57] A simple, rigid representation for the solutes, we therefore adopted planar geometries for DPB and the stilbene portions of HMS.

The methanol group in HMS also possesses conformational freedom. The minimum energy structure found using the AM1 model is one in which the OH bond is bent back toward the stilbene moiety (labeled "HMS" in Figure 1). The preference of this form over the "extended" form, shown as "HMS-ext" in Figure 1 is 10 kJ/mol based on AM1 calculations. However, this preference might be expected to weaken or reverse in solution, especially in the presence of strong hydrogen bonding
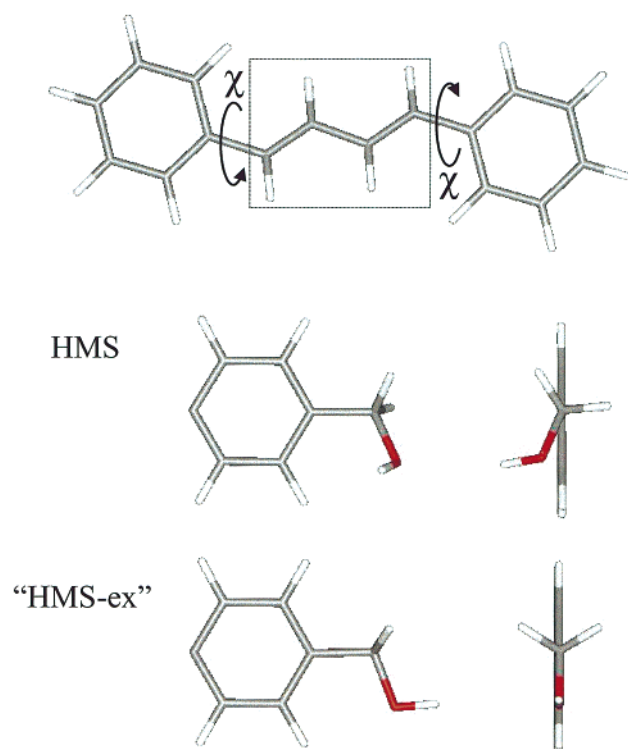
Figure 1. Structural features of DPB and HMS. The structures labeled "HMS" and "HMS-ex" show the benzyl portion of the HMS molecule in the conformation used in simulation (HMS) and in the higher-energy, extended form (HMS-ex).
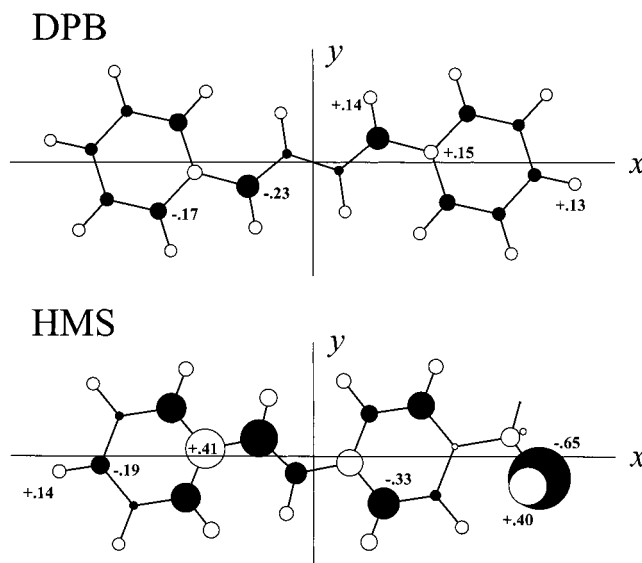

Figure 2. Illustration of the charge distributions of DPB and HMS. The circles represent the (ESP-fit) charges used in the simulation. The radius of these circles is proportional to the magnitude of the charge. Filled circles indicate negative values. (Only select charge values are shown here; see Supporting Information, Table 1 for a complete listing.) Also indicated are the principal inertial axes of these molecules.

partners. (On the basis of accessibility, the conformation labeled "HMS" would be preferred by H-bond donors whereas the extended form might be preferred by H-bond acceptors.) The model of HMS used in this paper is completely rigid with the geometry labeled "HMS" in Figure 1. To investigate the effect that choosing this particular conformer might have on the results, we also performed simulations at several densities using the "HMS-ext" form. Although the details of the solvent structure near the OH group differ slightly in these two cases, no significant differences in the extent of density augmentation or in the simulated rotational dynamics was observed.

Figure 2 depicts the charge distributions of DPB and HMS obtained from electrostatic potential fits[58] of 6-31G(d,p) wave functions (at the planar geometries). It should be noted that there are significant charges in both molecules, charges which lead to nonnegligible electrical interactions with CO_2. In addition to the net dipole moment of 1.8 D in HMS, which is created primarily by the OH bond moment ($\sim$1.9 D), the ring charges are also considerably larger in HMS than they are in DPB. We also note that the calculated dipole moment of HMS is much smaller than the experimental value of 2.9 $\pm$ 0.1 D measured in solution by Wiemers and Kauffman.[35] The source of this $\sim$1 D disagreement is not known. The calculated moment does depend somewhat on conformation (the value is 1.9 for the

HMS-ext geometry); however, the reported value of 2.9 D is higher than values calculated in any conformation. It is also higher than experimental values reported for comparable molecules,[59] for example benzyl alcohol has a dipole moment of 1.70$\pm$0.01 D in the gas phase and 1.6−1.7 D in benzene solution.[59]

Finally, Table 1 summarizes some of the geometric characteristics relevant to the rotational behavior of the two solutes. I_{xx}, I_{yy}, and I_{zz} are the principal moments of inertial. (The principal axis directions x, y, and z are defined in Figure 2.) As indicated by the fact that the values of Ray's asymmetry parameter (κ) are nearly −1, both molecules are close to the prolate limit.[60] The individual inertial components are quite similar, within 12%, in the two molecules. Also similar are the molecular lengths L_x, L_y, and L_z along the three principal axes. Because these inertial moments and lengths govern the rotational dynamics in the inertial and diffusive limits, this similarity suggests that the two molecules would display very similar rotational dynamics were it not for the difference in their electrical characteristics. It is for this reason that Kauffman and co-workers have selected this pair for studies of the effect of "dielectric friction" on rotational dynamics.[35]

III. Simulation and Experimental Procedures

Simulations were carried out in the microcanonical (NVE) ensemble at a series of densities spanning the range 0.2ρ_c to 2ρ_c, where ρ_c is the critical density (0.466 g cm^{-3} or 10.6 mol dm^{-3} for CO_2[61]). Total energies were chosen such that the

TABLE 1: Molecular Characteristics of DPB and HMS[a]

solute	formula	mass /amu	I_{xx} /amu·Å^2	I_{yy} /amu·Å^2	I_{zz} /amu·Å^2	κ	L_x/Å	L_y/Å	L_z/Å	μ/D
DPB	$C_{16}H_{14}$	206	198	3429	3627	−0.993	16.3	7.2	3.6	0
HMS	$C_{15}H_{14}O$	210	205	3030	3223	−0.991	15.5	7.2	4.2	1.8

[a] All properties refer to the planar conjugated systems and the "bent" HMS structure (see text) used in simulation. These geometries are based on AM1 optimizations. I_{xx}, I_{yy}, and I_{zz} are the moments of inertia, κ is Ray's asymmetry parameter,[60] and L_x, L_y, and L_z are molecular lengths (defined as the largest atom−atom separation plus the LJ radii of these atoms) along the principal coordinate directions. μ is the dipole moment obtained from MP2/6-31G(d,p) calculations.

Solvation and Friction in Supercritical Fluids

J. Phys. Chem. B, Vol. 106, No. 28, 2002 **7099**

average kinetic energies corresponded to temperatures of 311 ± 4 K, or about 7 K above the critical point of CO_2 ($T/T_c \approx$ 1.02). The systems simulated consisted of a single solute molecule and 860 solvent molecules. Cubic periodic boundary conditions were applied and all minimum image interactions summed (effective cutoffs were therefore roughly half of the unit cell length or greater than 20 Å in all cases). The equations of motion were integrated with a time step of 2 fs using a Verlet leapfrog scheme together with a rotational algorithm specific for linear-molecules for the solvent and a quaternion algorithm for the solute.[62] Simulations were started from crystalline lattice configurations and were equilibrated for 1 ns before collecting data for a period of 4 ns. As a check on the procedures employed here, we also ran simulations at a single density (0.63 ρ_c) in the NPT ensemble and using the Ewald method for treating the long-range electrical interactions.[63] To within statistical uncertainties, these alternative choices of ensemble and long-range correction had no effect on the static and dynamic quantities reported here.

Given our proximity to the solvent critical point it is also appropriate to ask whether systems consisting of 860 solvent molecules are sufficiently large for our purposes. Correlation lengths measured via X-ray scattering in CO_2 are less than 15 Å under all of the conditions simulated here.[64] At near-critical densities our simulation cell length is ~50 Å, or roughly 3 times this fluctuation length scale. In this situation, it seems likely that we are truncating the spectrum of fluctuations accessible to the system, at least to some degree. The extent to which the solute-centered properties of interest here are coupled to these large solvent fluctuations is not known. However, size-dependent simulations using atomic solvents[65] suggest that, at least for properties such as the number of solvent molecules in the 1st solvation shell and the solvation energy, the present systems provide values within ~10% of their values in the infinite-system limit.

The experimental data and analysis methods used to measure effective local densities for comparison to simulation follow the methods described in detail in ref 9 and will not be repeated here. DPB (98%) and HMS were obtained from Aldrich and were recrystallized twice from hexane prior to use. Electronic absorption spectra were recorded on a Hitachi U-3000 spectrometer using the spectroscopic cells and thermostating procedures previously described.[9] The CO_2 used was SCF grade (99.99%) obtained from Scott Specialty Gases. The spectral data reported here combine data from two independent sets of measurements for each solute.

IV. Results and Discussion

A. Solvation Structure. We begin by examining the solvation structure of DPB and HMS in CO_2. Because the results obtained for both solutes are similar, we will use DPB data for illustration purposes and discuss HMS only in terms of the small differences it displays compared to DPB.

Figure 3 shows snapshots of the near neighborhood of DPB at four CO_2 densities. These snapshots, and the corresponding movies of the time-dependent trajectories from which they are taken, provide a visual appreciation for the nature of solvation at the different densities explored here. At the lowest density studied, $0.25\rho_c$, the environment is that of a high-density gas. The solute encounters solvent molecules relatively frequently (>2 ps^{-1}) but the encounters are sufficiently separated to be largely independent. The number of solvent molecules in the immediate vicinity of the solute fluctuates widely, such that there are periods of a few picoseconds in which the solute is relatively
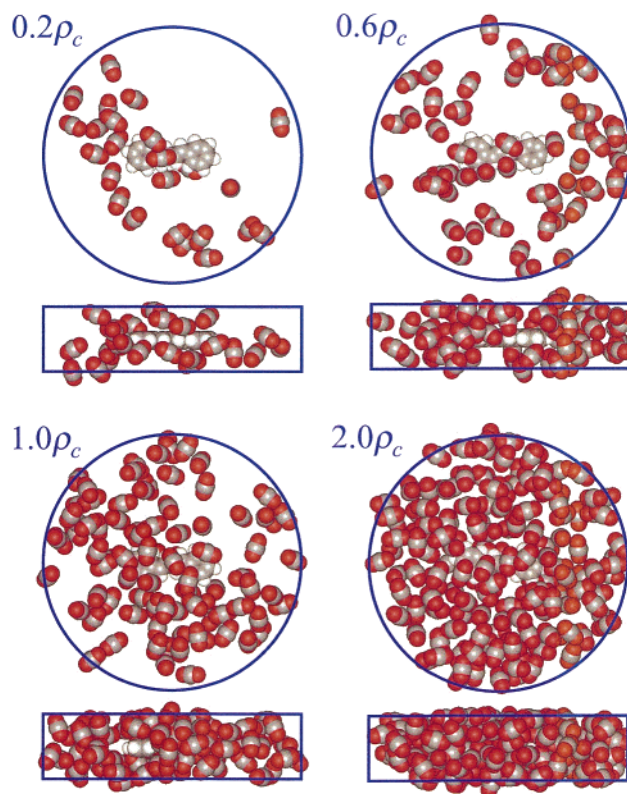

Figure 3. Snapshots of the region surrounding the solute from DPB/CO_2 trajectories at four solvent densities: 0.25, 0.63, 1.05, and 2.00 ρ_c.

free from the influence of solvent molecules, and similar lengths of time when it is a more dense environment. At densities approaching ρ_c, there are enough solvent molecules near to the solute that it is never free of significant interactions. As will be shown later, frequent solvent−solvent interactions at these densities spoil the independence of solute−solvent interactions. Finally, at the highest density studied, $2\rho_c$, the solute is in an environment much like that of an ordinary liquid solvent. The density is roughly 25% less than in typical solvents, which means that there is more free volume available in the high-density supercritical fluid. However, solvent molecules are also smaller, and therefore move more rapidly than in room-temperature liquid solvents, and it is therefore reasonable to assume that the solute surroundings are effectively homogeneous in the same sense they are in liquids. A final aspect to be noted from Figure 3 is that the build-up of solvent around the solute, i.e., density augmentation, is not large enough to be noticeable from visual inspection alone.

That substantial density augmentation is indeed present in these systems is better displayed in time-averaged data of the sort shown in Figures 4 and 5. Figure 4 depicts the average density of solvent atoms (either C or O) in the vicinity of the solute at the lowest and highest densities studied. Figure 5 shows reduced representations of such data at a series of densities using what we term "solvation shell distribution functions", $g_{ss}(r)$. These functions describe the relative probability of finding a solvent atom a distance r away from the nearest solute atom.[66] As such, they reflect the variation in solvent density as one moves outward from the surface of the solute, i.e., they summarize the shell-like solvation structure shown in Figure 4 averaged over the solute's surface. (These functions are comparable to the usual radial distribution functions used to describe the solvation structure of a spherical solute, but are more useful for solutes of arbitrary shape.)
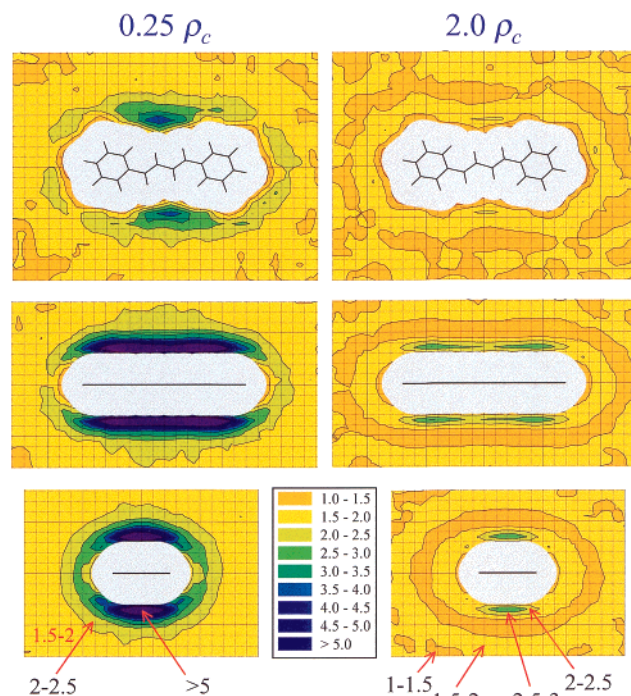
Figure 4.   Contour plots of the average relative densities of solvent atoms observed in the DPB/CO$_2$ system at the lowest and highest densities simulated. Densities are normalized by the bulk solvent density. Contours levels are as indicated. (The value of the background density in the $0.25\rho_c$ system is in the range $1-2$ over the region depicted.) Grid lines are at 1 Å intervals.
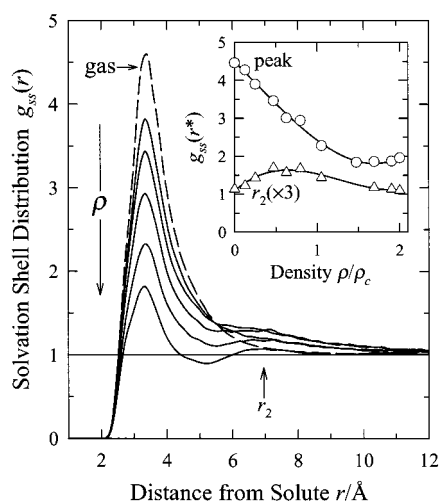

Figure 5.   "Solvation shell distribution functions" $g_{ss}(r)$ of the DPB/CO$_2$ system in the dilute gas limit (dashed curve) and at five solvent densities: 0.25, 0.47, 0.80, 1.05, and 1.90 ρ_c. $g_{ss}(r)$ is defined as the probability of finding a solvent atom at a distance r away from the nearest solute atom relative to a random distribution. The inset shows the density dependence of the maximum value of $g_{ss}(r)$ and the value at the 2nd-solvation shell maximum, is labeled r_2 in the figure. To make the variation in $g_{ss}(r_2)$ visible the difference between $g_{ss}(r_2)$ and 1 has been enlarged by a factor of 3 in this plot.

From Figure 5, we find that $g_{ss}(r)$ shows a main peak at ~3.2 Å, the average solute−solvent contact distance. The magnitude of this peak is greatest in the dilute gas limit ($\rho\rightarrow 0$). Here, the probability of finding a solvent atom "in contact" with the solute is 4−5 times greater than random, a value which reflects the fact that the average solute−solvent pair potential has a well depth of ~$1.5k_BT = 4$ kJ/mol.[66] Figure 4 (0.25 ρ_c) shows that this density is not uniform over the surface of the solute. Rather,
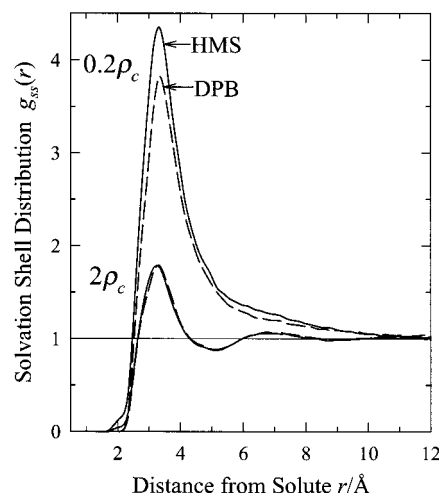

Figure 6.   Comparison of the solvation shell distribution functions g_{ss}-(r) of DPB/CO$_2$ (dashed curves) and HMS/CO$_2$ (solid curves) at the highest (2.00 ρ_c) and lowest (0.25 ρ_c) densities simulated.

it is concentrated mainly above and below the aromatic plane, where the solute−solvent interactions are most attractive. As density is increased from this low-density limit, g$_{max}$ decreases (inset of Figure 5) which means that compared to the bulk fluid, the *relative probability* of finding solvent atoms in close proximity to the solute decreases. (In contrast, the *number* of solvent atoms near the solute monotonically increases with increasing solvent density.) Thus, as one proceeds from the low-density regime, where solute−solvent attractions dictate structure, to the high-density ($\rho \approx 2\rho_c$) regime where packing considerations predominate (as signaled by the oscillatory shell structure seen in both figures) the density enhancement around the solute monotonically decreases. It is noteworthy that there is no obvious sign that proximity to the critical density is important in determining the makeup of the 1st solvation shell. However, it is also the case that these distribution functions develop long-range tails at intermediate densities due to the large correlation lengths in the vicinity of ρ_c. These solvent−solvent correlations do affect the solvation structure at larger distances, as can be seen from the fact that the variation of $g_{ss}(r_2)$, where r_2 is the distance of the 2nd solvation shell, exhibits a maximum at intermediate densities.

The density-dependence of the solvation structure and energetics of HMS in CO$_2$ is similar to that of the DPB/CO$_2$ system. This similarity is illustrated in Figure 6 and in the data summarized Table 2. In Figure 6, we compare the solvation shell distribution functions of HMS and DPB at the highest and lowest simulated densities. At $2\rho_c$ the two distributions are nearly identical. At $0.25\rho_c$ the relative solvent density around HMS is uniformly higher, however, the difference is small. In energetic terms, the difference in the heights of the two $g_{ss}(r)$ functions amounts to only about 0.1 k_BT. Density distributions of the sort shown in Figure 4 for DPB are also similar for the HMS solute. At the lowest densities, there is an increased density in the vicinity of the OH group in HMS, but the main enhancement is above and below the π system, just as in DPB.

Table 2 collects some statistics related to the coordination numbers and the energetics of solute−solvent interactions in both systems. The values N_1 and N_{1-2} are the average numbers of solvent atoms within the 1st and 1st + 2nd solvation shells, as determined by integration of $g_{ss}(r)$ out to distances of the 1st and 2nd minima observed at high densities. Note how little these coordination numbers differ between the two solutes. In both cases, they reflect 1st (1st + 2nd) solvation shell popula-

Solvation and Friction in Supercritical Fluids

J. Phys. Chem. B, Vol. 106, No. 28, 2002 **7101**

TABLE 2: Static Solvation Properties[a]

density /ρ_c	N_1	N_{1-2}	$-U$ /kJ mol^{-1}	$-U_{LJ}$ /kJ mol^{-1}	f_{El}	$\Delta\nu_{\#1}$ /cm^{-1}	$\Delta\nu_{\#2}$ /cm^{-1}
			DPB solute				
0.25	20	53	31.1	27.4	0.12	128	574
0.47	35	101	51.7	45.9	0.11	218	972
0.63	41	126	60.4	53.8	0.11	257	1140
0.80	45	140	65.6	58.4	0.11	277	1220
1.05	55	187	79.3	71.0	0.10	345	1520
1.48	64	236	92.0	83.0	0.10	406	1760
1.69	71	265	101.	91.2	0.10	445	1930
1.90	77	292	109.	98.6	0.10	486	2090
2.00	80	306	113.	102.	0.10	506	2170
			HMS solute				
0.25	22	55	36.2	29.6	0.18	122	560
0.63	42	126	65.5	54.3	0.17	226	1010
1.05	54	183	83.5	69.7	0.16	293	1300
1.69	69	257	105.	88.3	0.16	377	1640
2.00	79	299	120.	100.	0.16	433	1860

[a] N_1 and N_{1-2} are the numbers of solvent *atoms* in the 1st and 1st + 2nd solvation shells, respectively. These shells are defined by the distance between a solvent atom and the nearest solute atom being $\leq$ 5 Å and $\leq$ 9 Å, respectively. (The number of solvent molecules are very close to 1/3 of these atom numbers.[67]) U is average interaction energy between the solute and solvent. U_{LJ} is the energy contributed by Lennard-Jones interactions and f_{El} is the fraction of the total energy contributed by electrical interactions. $\Delta\nu_{\#1}$ and $\Delta\nu_{\#2}$ are frequency shifts ($\nu_{soln}-\nu_{gas}$) calculated by two different approaches, as described in the text (eqs 2 and 5). Statistical uncertainties in these static averages, defined by the standard deviations of the mean of 10 runs of 400 ps each, are typically less than 2% at densities below ρ_c and less than 1% at higher densities.

tions that range between approximately 7 (18) CO_2 molecules at the lowest density to 27 (100) molecules at $2\rho_c$ ($N_{mols} \cong N_{atoms}/3$[67]). The solute−solvent interaction energies U are also similar in the two systems, with the interactions between HMS and CO_2 being 5−10% more attractive than those between DBP and CO_2 at most densities. In both cases, the interaction energy per molecule in the 1st solvation shell is between 4 and 5 kJ/mol, roughly the average interaction energy of isolated solute−solvent pairs. The main difference in the solvation energetics of DPB and HMS lies in the greater electrical interactions between HMS and the quadrupolar CO_2 solvent molecules. As shown by the column labeled "f_{el}" in Table 2, a significantly larger fraction of the total solute−solvent interaction comes from electrical interactions in the HMS case. However, in both solutes, electrical interactions make up only a minor fraction, always less than 20%, of the total interaction energy.

As a final aspect of solvation structure, we consider the importance of hydrogen bonding between HMS and CO_2. As mentioned in the Introduction, Anderton and Kauffman[19] proposed that the origin of the slower rotation observed for HMS compared to DPB lies in the ability of HMS to form hydrogen bonds with CO_2. However, we do not find evidence for such hydrogen bonding being of much importance in the simulated systems. Atom−atom radial distribution functions of the HMS−CO_2 system do not reveal any structurally distinctive associations between the OH group of HMS and CO_2 under the conditions of the simulations. We find only a small peak (g_{max} < 1.5) at short distances (∼2.2 Å) in the $(O_u)H_v$ - - - O_v distribution indicative of H-bond donation by HMS to CO_2. The radial distribution functions are not highly structured, rather they appear to indicate the presence of many different arrangements of solvent molecules around the OH site. Snapshots such as those shown in Figure 3 also fail to reveal any special interactions with the OH group.

To explore the idea of hydrogen bonding further, we examined the nature of the HMS−CO_2 pair potential, using a
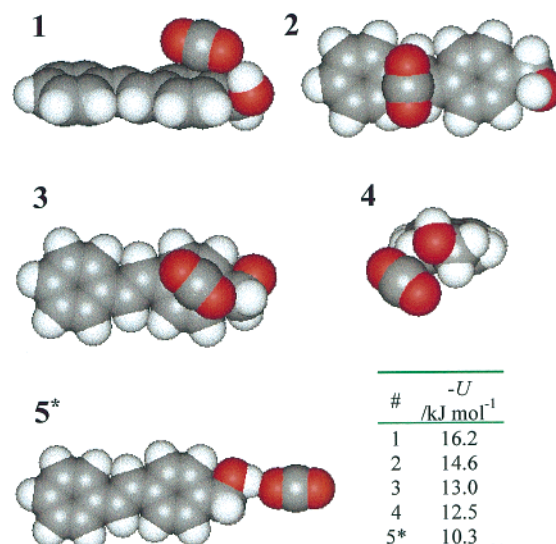

#	$-U$ /kJ mol^{-1}
1	16.2
2	14.6
3	13.0
4	12.5
5*	10.3

Figure 7. Sample low energy structures of the HMS − CO_2 potential surface and their corresponding energies. The structures depicted are representative of the different classes of complexes observed, however, there are many other nearly isoenergetic minima, for example having structures such as #2 and #3 but on opposite sides of the aromatic plane. Structures #1−4 involve the HMS conformer used in most of the simulations. Structure #5* involves the alternative "HMS-ext" conformer discussed in connection with Figure 1.

Monte Carlo minimization algorithm[68] to find local minima on the potential energy surface. Some of the lowest energy structures found in this way are depicted in Figure 7. The global minimum is indeed a distorted ($\angle O_u-H_u-O_v = 154°$) hydrogen bonded structure, the structure labeled #1 in Figure 7. However, in addition to this global minimum, there are many other local minima having only slightly higher energies. For example, within 2−3 kJ/mol of the global minimum there are many minima, represented by structures #2 and #3, in which the CO_2 molecule interacts with the aromatic system of HMS. Under supercritical conditions, these non-hydrogen-bonding minima are within 1−2 k_BT of the hydrogen bonded structure, and they are much more numerous. It is therefore not surprising that the hydrogen-bonded structure does not show up with any special prominence in the simulations. On the basis of these calculations, we conclude that, although hydrogen bonding does occur between HMS and CO_2, this interaction is not likely to significantly alter the behavior of HMS/CO_2 compared to what would be observed in its absence.[69] The small differences observed between HMS and DPB (Figure 6), although electrical in origin, do not appear to be directly related to hydrogen bonding. Examination of the DPB/CO_2 potential energy surface shows similar π-system − CO_2 interactions as in HMS. These interactions are slightly weaker in DPB/CO_2, averaging 13.6 kJ/mol. The difference, which is also the primary reason HMS shows slightly greater density enhancement than DPB, lies in the larger π-system charges in HMS compared to DPB (Figure 2). In the absence of charges, the π-bonded solute − CO_2 interaction energies are substantially lower, and essentially the same in the two systems (∼9.8 kJ/mol).

B. Experimental and Simulated Spectral Shifts and Density Augmentation. To provide comparisons to the structural and energetic results obtained from simulation, we have measured the shifts in the electronic absorption spectra of DPB and HMS in supercritical CO_2 as well as in the gas phase and in liquid solvents. Figure 8 shows sample experimental data for the case of DPB. We will compare such data to the results of simulation in two ways: (i) by modeling spectral shifts using
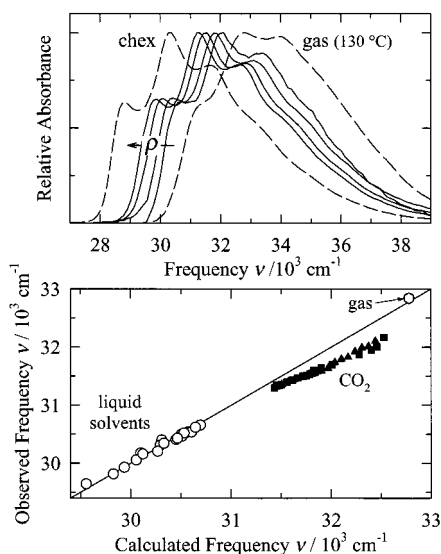
Figure 8. Representative solvatochromic data of the sort used to determine effective local densities from experiment. The data here are for the DPB solute. The top panel shows normalized absorption spectra in the gas phase and in a typical liquid solvent, cyclohexane ("chex"; dashed curves). The solid curves are spectra in supercritical CO_2 at 306 K and densities of 0.5, 1.0, 1.5 and 2.0 ρ_c in the order indicated. The bottom panel shows the correlation of the frequencies of the DPB absorption spectrum in the gas-phase and in 20 liquid solvents (open symbols) using eq 2. The filled symbols show corresponding data from two independent measurements of DPB in supercritical CO_2.

simulation data for direct comparison to experimental shifts and (ii) by using the methods commonly applied[9,70] to deduce effective local densities from the experimental data and comparing these values to simulated coordination numbers. Exploring the relationship between these two approaches provides insights into the meaning of the values of density augmentation reported in experimental studies.

We first consider the direct simulation of spectral shifts. As accurate prediction of such shifts is still beyond the reach of current electronic structure methods, we instead use two distinct semiempirical approaches that have previously been employed for modeling the spectra of jet cooled complexes.[71,72] Without adjustment, neither model accurately reproduces the *magnitudes* of the shifts observed in experiment. Nevertheless, they should provide plausible and distinct predictions for the *density dependence* of the shift, which is of main interest here. In both cases, we ignore possible dynamical effects[73] and assume that the electronic spectra reflect merely the distribution of $S_0 - S_1$ energy differences observed during the course of simulations of the S_0 trajectories.

The first model relates solvent-dependent shifts to differences in the solute's Lennard–Jones parameters in the S_0 and S_1 states. Specifically, we assume that the Lennard–Jones well depth parameter ϵ_{CC} of the carbon atoms involved in the electronic transition (i.e., all of the sp^2 carbons) uniformly increase by 10% in S_1 compared to S_0. The shift in this case is given by

$$h\Delta\nu_{\#1} = \sum_{i=1}^{N_a}\sum_{\beta=1}^{n_C} 4\Delta\epsilon_{i\beta}\left\{\left(\frac{\sigma_{i\beta}}{r_{i\beta}}\right)^{12} - \left(\frac{\sigma_{i\beta}}{r_{i\beta}}\right)^{6}\right\}$$

$$\Delta\epsilon_{i\beta} = 0.0488\sqrt{\epsilon_{ii}\epsilon_{\beta\beta}} \quad (2)$$

where the index i refers to solvent atoms and β to the relevant carbon atoms of the solute. The choice $\Delta\epsilon_{\beta\beta} \equiv \epsilon_{\beta\beta}(S_1) - \epsilon_{\beta\beta}(S_0) = 0.1\epsilon_{\beta\beta}(S_0)$ is somewhat arbitrary, but it is comparable to

the values that have been successfully used to match aromatic-rare gas cluster spectra.[71,72]

The second model derives from a treatment of dispersive solvent shifts by Shalev et al.[74] Here, a 2nd-order perturbation expansion of the solute–solvent interaction energy in the basis of solute molecular orbitals predicts that the spectral shift can be written

$$h\Delta\nu_{\#2} = \sum_{i=1}^{N_a}\alpha_i e^2\bar{F}_i\sum_{\beta=1}^{n_C}\sum_{\gamma=1}^{n_C}K_{\beta\gamma}^{(i)}G_{\beta\gamma}^{(i)} \text{ with } G_{\beta\gamma}^{(i)} = \frac{\vec{r}_{i\beta}\cdot\vec{r}_{i\gamma}}{r_{i\beta}^3 r_{i\gamma}^3} \quad (3)$$

In this expression, i again refers to solvent atoms, β and γ refer to solute atoms, and α_i and $\bar{F}_i$ are the electronic polarizability and ionization potential of solvent atom i. Information about the electronic transition is contained in the factor $K_{\beta\gamma}^{(i)}$, which involves sums over many energy-weighted molecular orbital coefficients. We greatly simplify the calculations by assuming that these sums can be replaced by the single term involving only orbitals explicitly involved in the electronic excitation. In DPB and HMS, the $S_0{\rightarrow}S_1$ transition is reasonably described as a single $\pi\pi^*$ HOMO → LUMO excitation.[75] $K_{\beta\gamma}^{(i)}$ can therefore be approximated

$$K_{\beta\gamma}^{(i)} \cong \frac{Q_\beta Q_\gamma}{\epsilon^{\text{LUMO}} - \epsilon^{\text{HOMO}} - \bar{F}_i} \cong \frac{Q_\beta Q_\gamma}{h\nu_{\text{gas}} - \bar{F}_i} \quad (4)$$

where Q_β and Q_γ are the transition monopoles $Q_\beta = C_\beta^{\text{HOMO}}C_\beta^{\text{LUMO}}$ on solute atoms β and γ. We also treat the atoms of the CO_2 solvent molecules as independent sites for polarizability interaction, with the polarizability of each atom being 1/3 that of the entire molecule. The expression for the spectral shift can then finally be written

$$h\Delta\nu_{\#2} \cong fe^2\sum_{i=1}^{N_a}\sum_{\beta=1}^{n_C}\sum_{\gamma=1}^{n_C}Q_\beta Q_\gamma\frac{\vec{r}_{i\beta}\cdot\vec{r}_{i\gamma}}{r_{i\beta}^3 r_{i\gamma}^3} \quad (5)$$

with the value of $f \cong \alpha\bar{F}/3(h\nu_{\text{gas}} - \bar{F}) = 1.2$ Å^3 being used for simulation. (The transition monopole values derived from AM1/CI calculations[75] are provided in Supporting Information, Table 1.)

The results of both of these spectral shift calculations are compared to experimental data in the top panels of Figures 9 and 10. All shifts are shown normalized to their value $\Delta\nu_{\text{ref}}$ at a reference density of $2\rho_c$. The normalization factors are tabulated in the inset to the figures. Considering first these reference shifts, one notes that the observed shift is about 40% larger in DPB than in HMS. Both models correctly predict the DPB shift to be larger, but both models predict less of a distinction between the two solutes than is observed experimentally. The actual magnitudes of the shifts predicted by model #1 are 50–70% too high, whereas model #2 predicts shifts that are more than a factor of 2 small. Although the magnitudes of the calculated shifts are far from the experimental values, the physical models underlying these calculations are reasonable enough to provide useful predictions of the density dependence expected for the shifts. As shown in Figures 9 and 10, the variations with density are nearly identical in the two models. Both model curves lie close to the experimental points; however, the nonlinearity of the experimental $\Delta\nu$ versus ρ plots are slightly underestimated in both systems. This departure from a linear density dependence is what is used to experimentally measure the extent of local density augmentation in the solute's
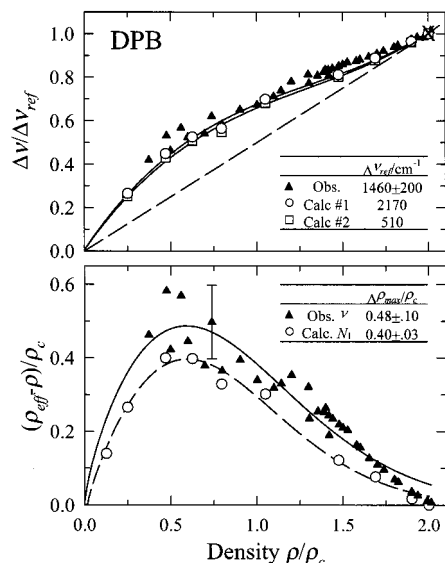
Solvation and Friction in Supercritical Fluids

J. Phys. Chem. B, Vol. 106, No. 28, 2002 **7103**

Figure 9. Comparison between experimental and simulated frequencies (top) and estimates of density augmentation (bottom) for the system DPB/CO_2. The top panel shows spectral shifts from the gas phase $\Delta \nu = \nu_{gas} - \nu$ normalized to the shift observed at a reference density of $2\rho_c$. The values used for normalization are listed in the table insert. (See text for a description of the calculations.) The bottom panel shows the "density augmentation", the difference between the effective local density and the bulk density, $\Delta \rho \equiv \rho_{eff} - \rho$. Observed augmentation values are deduced from electronic frequency shifts and a dielectric continuum analysis. Calculated values are determined from the number of solvent atoms in the 1st coordination shell (N_1). Both measures of density are defined such that $\Delta \rho = 0$ at a reference density of $\rho_{ref} = 2\rho_c$. The table inserted in the bottom panel shows the estimates of the maximum value of $\Delta \rho$. In both panels, the curves drawn through the data are only intended as a visual guide.
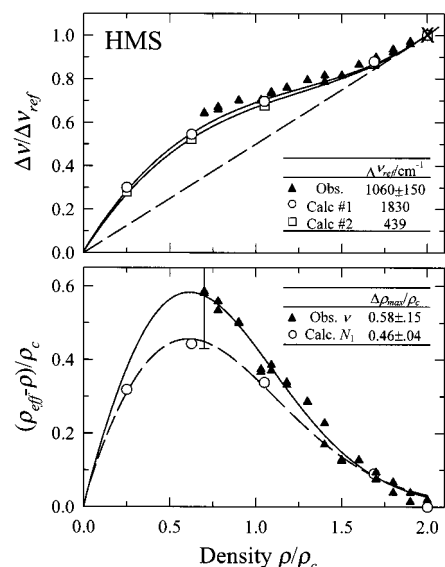

Figure 10. Comparison between experimental and simulated frequencies (top) and estimates of density augmentation (bottom) for the system HMS/CO_2. See caption to Figure 9 for details.

neighborhood. We therefore next consider such experimental estimates of local densities and how they compare to simulated quantities.

The method we employ for determining effective densities ρ_{eff} from experimental spectral shifts[76] has been thoroughly documented in ref 9. Here, we only need mention the two key

assumptions upon which the analysis rests. One assumption is that data from the gas phase and a series of liquid solvents can be fit to a dielectric model of solvatochromism and this fit used to calibrate the behavior expected in the absence of density augmentation. Such a fit is shown in the bottom panel of Figure 8. The second assumption is that at a reference density of $2\rho_c$ the solvation environment in a supercritical fluid is comparable to that in a dense liquid solvent, a condition we define to have zero density augmentation, i.e., $\rho_{eff} = \rho$ at $\rho = 2\rho_c$. It is important to note that by virtue of this definition, "density augmentation" refers specifically to the excess solvent density in the vicinity of a solute that results from attractive interactions in the compressible regime of a supercritical fluid. This augmentation excludes the excess density present in liquid solvents and in supercritical solvents at high densities (i.e., at $2\rho_c$) due to packing considerations.

Effective local densities are derived by first fitting spectral data in liquid solvents and in the gas phase to the relation

$$\nu = \nu_0 + \alpha f(n^2) + \beta f(\epsilon) \text{ where } f(x) = \frac{x-1}{x+2} \quad (6)$$

where n is the refractive index and ϵ the dielectric constant of the solvent. DPB and HMS frequencies in 20 liquid solvents and in the gas phase (data available as Supporting Information, Table 2) in this manner yield the following correlations

$$\text{DPB: } \nu/10^3 \text{ cm}^{-1} = 32.78 - 9.250 f(n^2) - 0.354 f(\epsilon)$$
$$(\delta = 0.05) \quad (7a)$$

$$\text{HMS: } \nu/10^3 \text{ cm}^{-1} = 35.36 - 7.213 f(n^2) - 0.197 f(\epsilon)$$
$$(\delta = 0.06) \quad (7b)$$

where δ is the standard error of the fit. As illustrated in Figure 8, such correlations provide an accurate representation of the spectral frequencies in all solvents studied, solvents which span a wide range of polarities and functional groups. The small value of β relative to α indicates that the spectral shifts of both solutes are dominated by interactions with the solvent's electronic polarizability, as opposed to interactions with its permanent electrical moments. (Both of the spectral shift models described above, eqs 2 and 5, assume that such nonpolar mechanisms are solely responsible for the spectral shift.) We note that these correlations reproduce the frequencies of both solutes in high-density ($\sim 2\rho_c$) CO_2 to within the statistical uncertainties. Using these fits, together with the known density dependence of n and ϵ of CO_2, and the assumption of zero density augmentation at $2\rho_c$, the observed frequencies in CO_2 are converted to effective local densities or to values of the density augmentation $\Delta \rho_{eff}^{\nu_{obs}} \equiv \rho_{eff}(\nu_{obs}) - \rho$.[77]

The experimental estimates of $\Delta \rho_{eff}^{\nu_{obs}}$ are shown as the filled points in the bottom panels of Figures 9 and 10. The effective excess densities deduced from experiment are maximal at a (bulk) solvent density of roughly $0.6\rho_c$, consistent with the behavior observed in a wide range of systems.[9,10] The maximum magnitude of this excess is $(0.48\pm0.10)\rho_c$ in DPB and $(0.58\pm0.15)\rho_c$ in HMS. (Estimated uncertainties in these numbers reflect both the reproducibility of the experimental frequencies as well as other uncertainties in the analysis.[9]) The data suggest that the effective augmentation surrounding the HMS solute is slightly greater than in the case of DPB, however, the difference is within estimated uncertainties.

We compare these experimental results to values determined from the coordination numbers N_1 observed in simulation by defining

$$\Delta\rho_{\text{eff}}^{(N_1)} = \rho_{\text{eff}}^{(N_1)} - \rho \equiv \frac{N_1(\rho)}{N_1(\rho_{\text{ref}})}\rho_{\text{ref}} - \rho \qquad (8)$$

where again $\rho_{\text{ref}} = 2\rho_c$. Figures 9 and 10 show that the simulated density augmentation $\Delta\rho_{\text{eff}}^{(N_1)}$ closely parallels the experimental data. For example, the simulated curves are maximal at a density of $\sim 0.6\rho_c$ as in experiment. The maximum value of the augmentation deduced from simulation is also slightly larger in the HMS system $(0.46\pm0.03)\rho_c$ relative to DPB (0.40 ± 0.03)-ρ_c, as is found experimentally. Finally, the magnitude of the simulated density augmentation $\Delta\rho_{\text{eff}}^{(N_1)}$ is similar to, but slightly less than $\Delta\rho_{\text{eff}}^{\nu_{\text{obs}}}$ deduced from experiment. Because this difference in magnitude is smaller than the combined uncertainties in the two types of data, it would be reasonable to conclude that there is satisfactory agreement between simulation and experiment here. This agreement between $\Delta\rho_{\text{eff}}^{(N_1)}$ and $\Delta\rho_{\text{eff}}^{\nu_{\text{obs}}}$ is noteworthy in that it helps to substantiate the general notion that electronic spectral shifts report on solvent conditions in the 1st solvation shell of solutes such as DPB and HMS.

Despite this reasonable agreement, we believe that the $\sim$20% smaller density augmentation reported by the simulation compared experiment is significant and worthy of further comment. Rather than being an isolated result, the differences between simulation and experiment displayed in Figures 9 and 10 fit into a general pattern noted previously when comparing simulated and experimental estimates of augmentation.[10] When considering the possible origins of this difference, it should be kept in mind that spectral shifts are not (necessarily) directly related to coordination numbers so that there is no a priori reason $\Delta\rho_{\text{eff}}^{\nu_{\text{obs}}}$ and $\Delta\rho_{\text{eff}}^{(N_1)}$ should be identical.[78] However, to a good approximation, the shifts calculated using either spectral model described above are simply proportional to N_1. For this reason, if one were to calculate effective densities from either $\Delta\nu_{\#1}$ or $\Delta\nu_{\#2}$ using the same procedures applied to experimental data, they would produce $\Delta\rho_{\text{eff}}$ curves negligibly different from the $\Delta\rho_{\text{eff}}^{(N_1)}$ curves shown in Figures 9 and 10. Thus, direct comparison of $\Delta\rho_{\text{eff}}^{(N_1)}$ and $\Delta\rho_{\text{eff}}^{\nu_{\text{obs}}}$ is justified. The $\sim$20% smaller magnitude of $\Delta\rho_{\text{eff}}^{(N_1)}$ relative to $\Delta\rho_{\text{eff}}^{\nu_{\text{obs}}}$ curves is a direct reflection of the slight underestimation of the nonlinearity in $\Delta\nu(\rho)$ displayed in the top panels of Figures 9 and 10.

We distinguish two possible origins for this imperfect agreement between simulation and experiment. First, the simulations might underestimate the extent of density augmentation. As noted earlier, a study of system size dependence in monatomic solvents[65] suggests that, in the compressible regime, values of N_1 might be as much as 10% smaller in the present simulations compared to the infinite system limit. This system size effect would tend to reduce the extent of density augmentation observed in the simulations, and may account for some portion of the discrepancy observed here. Alternatively, it might be that the simulations accurately represent the local solvation structure, but that the models we have used to describe spectral shifts (both in experiment and in simulation) are incorrect in their density dependence. The models used in simulation assume complete additivity of the contributions from individual solvent molecules or solvent atoms. In reality, the dispersion interactions we represent via models #1 and #2 contain multibody contributions which are neglected in the present description.[79] The inclusion of such nonadditive effects breaks the proportionality between $\Delta\nu$ and N_1 and leads to larger departures from linearity in curves of $\Delta\nu$ versus ρ, which would help explain the differences observed. In simulations of anthracene in a monatomic solvent, treating this nonadditivity in the manner suggested
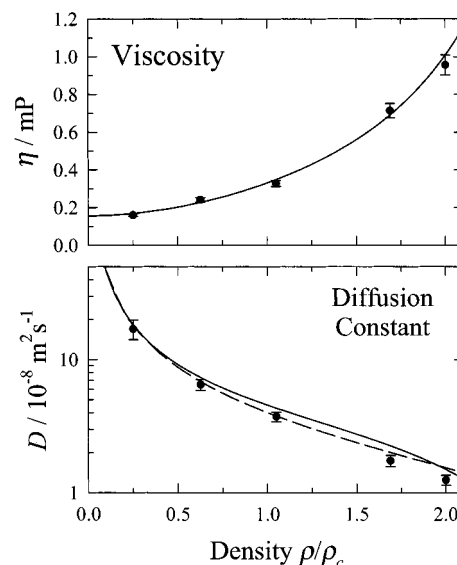

Figure 11. Simulated (points) and experimental (curves) shear viscosities and self-diffusion coefficients of neat CO_2 at 310 K. The experimental viscosity curve uses the correlating function of ref 111 and the two curves representing experimental diffusion coefficients are from refs 109 (solid) and 110 (dashed).

TABLE 3: Transport Properties of Neat CO_2 (310 K)[a]

density ρ/ρ_c	viscosity η/mP		diffusion constant $D/10^{-8}$ m^2 s^{-1}	
	sim	expt	sim	expt
0.25	$0.161 \pm .007$	0.17	17 ± 3	18/18
0.63	$0.241 \pm .012$	0.23	$6.5 \pm .6$	7.3/6.8
1.05	$0.33 \pm .02$	0.35	$3.7 \pm .3$	4.3/3.8
1.69	$0.71 \pm .04$	0.69	$1.7 \pm .2$	2.3/2.0
2.00	$0.96 \pm .05$	1.00	$1.3 \pm .2$	1.5/1.5

[a] Shear viscosities η and self-diffusion constants D calculated from 4 ns simulations of 860 or 864 CO_2 molecules. Uncertainties listed for η correspond to the standard error of the mean of 10 runs of 400 ps each. In the case of D, the uncertainty listed is twice the difference between the values calculated from the two components of eq 10. Experimental values of η were calculated using the correlating equations of Vesovic et al.[108] The two experimental values listed for D are from the parametrizations of refs 109 (left) and 110 (right). These correlations are reported to reproduce experimental data to within the variability of data from different laboratories, with mean average errors of $\pm$7% in η and $\pm$6% in D.

by Stratt and Adams,[80] leads to an increase in the apparent augmentation by on the order of 10%.[65] This latter explanation is likely to be the more important effect, but only further calculations on these systems will settle the issue. For now, we note that whatever the origin of the difference, it is small, and it is therefore reasonable to assume that the present simulations are fairly realistic in their depiction of solvation structure.

C. Dynamics: Experiment−Simulation Comparisons. Having considered the ability of the simulations to reproduce the static characteristics of these systems, we now turn to comparing simulated and observed dynamics. Before discussing the results for solute rotation, we first consider two transport properties that reflect the frictional characteristics of the pure solvent.

Figure 11 and Table 3 compare simulated and experimental values of the shear viscosity (η) and self-diffusion coefficient (D) of CO_2. The ability of the CO_2 model used here to reproduce these transport properties is relevant to the problem of solute rotation since both can be considered measures of solvent friction − viscosity within the context of hydrodynamic models
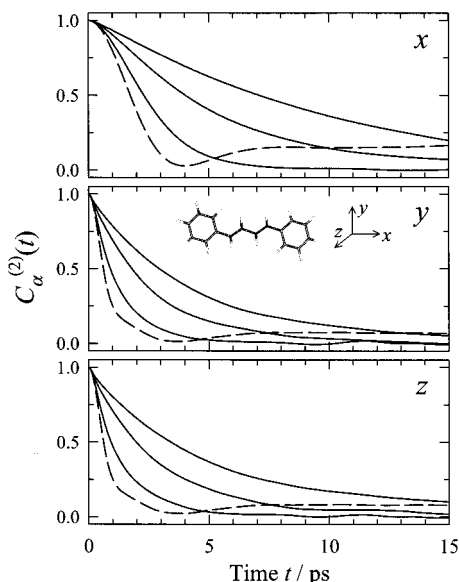
Solvation and Friction in Supercritical Fluids

J. Phys. Chem. B, Vol. 106, No. 28, 2002 **7105**

Figure 12. 2nd rank orientational correlation functions $C_\alpha^{(2)}(t)$ for rotation of the three principal axis directions $\alpha = x, y, z$ of DPB. Solid curves are simulation results at three densities, 0.25, 1.0, and 2.0ρ_c (bottom to top) and the dashed curves are the free rotor ($\rho = 0$) limit.

and D^{-1} as an empirical collision frequency appropriate over the entire gas-to-liquid density range.[81,82] These properties were determined from separate simulations of neat CO_2 systems using the relations[62]

$$\eta = \frac{V}{k_B T}\int_0^\infty \langle P_{\alpha\beta}(0)P_{\alpha\beta}(t)\rangle\, dt \qquad (9)$$

and

$$D = \frac{1}{3}\int_0^\infty \langle \vec{v}_i(0)\cdot\vec{v}_i(t)\rangle dt = \lim_{t\to\infty}\frac{\langle|\vec{r}_i(0)-\vec{r}_i(t)|^2\rangle}{6t} \qquad (10)$$

where $P_{\alpha\beta}$ is an off-diagonal element of the system pressure tensor and $\vec{v}_i$ and $\vec{r}_i$ are the center of mass velocity and position of molecule i and V the system volume.[83]

As shown in Figure 11, the calculated viscosities reproduce the experimental values to within the statistical uncertainties of the simulation. The calculated diffusion coefficients show the correct density dependence, but the magnitudes of D are systematically smaller than their experimental counterparts at higher densities, perhaps by as much as 20% at 2ρ_c. In addition to these transport properties, we also examined the rotational dynamics of CO_2 molecules in these neat fluid simulations. We also find good agreement between the simulated rotational correlation times and those deduced from light-scattering experiments.[84,85] Collectively, these comparisons show that the CO_2 model of Harris and Yung,[53] although parametrized solely on the basis of static properties, also provides a reasonable representation of the frictional characteristics pertinent to solute dynamics.

We therefore now turn to the simulated rotational dynamics of DPB and HMS in this model solvent. Representative orientational correlation functions

$$C_\alpha^{(L)}(t) = \langle P_L[\hat{u}_\alpha(0)\cdot\hat{u}_\alpha(t)]\rangle \quad P_1(x) = x,\ P_2(x) = \frac{3}{2}x^2 - \frac{1}{2} \quad (11)$$

for rotation of the three principal axis directions $\hat{u}_\alpha$, $\alpha = x, y, z$ of DPB are shown in Figure 12. The solid lines are data at
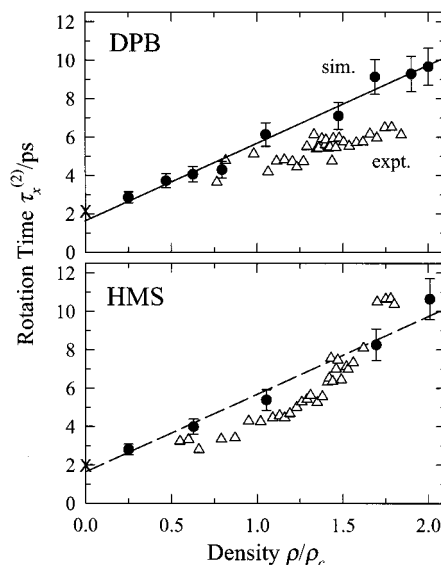

Figure 13. Orientational correlation times $\tau_x^{(2)}$ as a function of CO_2 density. Filled symbols and lines denote simulated data and open symbols are the experimental results of Anderton and Kaufffman.[19] The "X"s at $\rho = 0$ are the 1/e times of the free rotor correlation functions. The solid line in the top panel is a linear regression to all of the simulated DPB data (not $\rho = 0$). The dashed line in the bottom panel reproduces this DPB regression in order to show the approximate equality between the HMS and DPB times. The error bars in this figure are ±1 standard deviation of the mean of 10 data sets. Uncertainties in the experimental times were estimated to be ±0.8 ps or roughly the range of the scatter in these data.[19]

densities of 0.25, 1.0, and 2.0ρ_c and the dashed lines show the free rotor limit.[86] In Figure 12, we have plotted the 2nd rank functions for the DPB solute. The simulated 1st rank functions are qualitatively similar but a factor of 2–3 slower (see below). The HMS correlation functions are also comparable to those depicted in Figure 12. What such curves indicate is that for both solutes, rotation of the y and z axes occurs at nearly the same rate, whereas the rotation of the longest axis x is about a factor of 2 slower. Even at the lowest density studied, 0.25ρ_c, the rotational correlation functions depart significantly from the free rotor curves at times of less than 1 ps. This rapid departure reflects the fact that even at very low densities, solutes of this size undergo collisions (as measured by angular velocity correlation times, see below) at a rate of greater than 1 ps^{-1}. In most cases the initial Gaussian character of the free-rotor correlation functions is manifest in the observed $C_\alpha^{(L)}(t)$ only at times so short that little motion has occurred. Over more than 90% of their decay, most of these curves are well characterized as single-(x) or bi-(y,z) exponential functions of time (see below). At densities below 0.5ρ_c the reorientation of the experimentally observable x axis does depart sufficiently from an exponential decay so that one might be able to detect the difference experimentally (solubility and time-resolution permitting).

The data currently available from experiment are not the correlation functions themselves but rather the rotational correlation times of the x inertial axis[87]

$$\tau_x^{(2)} = \int_0^\infty C_x^{(2)}(t)dt \qquad (12)$$

Experimental rotation times, derived from analysis of steady-state fluorescence anisotropies by Anderton and Kauffman[19] are compared to simulated data in Figure 13. The correspondence

between the experimental and simulation data is poorer than might be expected in several respects. First, the simulated rotation times are generally larger than the experimental times. The difference is especially evident in the case of DPB at the higher densities ($1.5 \leq \rho/\rho_c \leq 1.8$) where the simulated times are as much as 30% larger than experiment. At such densities there is approximate agreement in the case of HMS but at lower densities there is again a significant discrepancy between the experimental and simulated times. The simulated rotation times are approximately linear functions of density, as indicated by the linear regression shown in the top panel of Figure 13. The experimental DPB might be considered to be linear in density, however, the HMS data are at least suggestive of a nonlinear density dependence. Finally, in their experimental study, Anderton and Kauffman[19] stressed the differences between the rotational dynamics of DPB and HMS in CO_2. In contrast, the simulated rotation times of the two solutes are the same to within uncertainties, as indicated by the dashed line in the bottom panel of Figure 13, which reproduces the DPB correlation line for comparison to the HMS points.

Of the differences displayed in Figure 13, of most concern is the fact that the simulated rotation times of DPB are ~30% larger than the observed times at the higher solvent densities. This deviation cannot be considered insignificant when one appreciates the fact that the *change* in rotation times from the low density limit to these high densities differs by nearly a factor of 2 between simulation and experiment. In attempting to reconcile this discrepancy, possible errors in both the simulations and the experiments can be considered. On the simulation side, one must always question the realism of the models employed. The fact that the CO_2 model nicely reproduces the experimental viscosities over the density range studied provides confidence in the solvent representation. That the solute–solvent interactions are also reasonably represented is indicated by the comparisons of spectral shifts and density augmentation made in the last section. If anything, the latter results indicate that the simulations may slightly underestimate the strength of solute–solvent interactions and therefore lead to an underestimation of the friction and rotation times compared to experiment. It should also be noted that the rotation times measured in experiment apply to the *excited-state solute,* whereas the ground-state solute is what is observed in absorption experiments and simulated here. However, the differences between the ground and excited state interactions with the solvent are expected to be modest and would likely be in such a direction as to once again lead the simulations to underestimate the rotational friction. It is therefore difficult to understand why the simulations should predict the rotation of DPB in CO_2 to be too slow by ~30%. We thus consider whether possible errors in the experimental data or analysis might be the source of the disagreement. An obvious candidate when using steady-state anisotropies to measure rotation times is depolarization due to window birefringence, which, if undetected will lead to an underestimation of rotation times. However, Anderton and Kauffman carefully checked for this artifact and found it to be negligible in their experimental setup.[19] A less obvious possibility is the use of an inaccurate value of the limiting anisotropy "r_0". Anderton and Kauffman used a value of $r_0 = 0.39$ in their analysis of DPB, the value was measured in glycerin at $-20\ °C$.[34] It is possible that this value is too high in supercritical CO_2, as a result of density-dependent changes in the mixing of the underlying 2^1A_g and 1^1B_u states that makeup S_1.[88] This state dependence on density is signaled by the large change in radiative rate from a value of $7.7 \times 10^8\ s^{-1}$

characteristic of the allowed 1^1B_u state in most liquid solvents[41] to the value of $1.5 \times 10^7\ s^{-1}$ in the gas phase where S_1 emission is dominated by the forbidden character of the 2^1A_g state.[89] It is not clear how this change in the allowed character of the transition might alter the value of r_0 appropriate to the supercritical CO_2 environment compared to that appropriate in liquid solution.[90] We note however, that reduction of the value from 0.39 to 0.30 would bring the experimental rotation times into excellent agreement with the simulations. Whether this is indeed the source of the disagreement in the case of DPB will have to await direct time-resolved measurements of rotation times.

The remaining differences between simulation and experiment, although not negligible, are more understandable, and at least partly a matter of interpretation. Thus, the simulated and experimental times of HMS are actually in reasonable agreement if one considers the combined uncertainties in the two data sets (± 0.8 ps in experiment[19]). We note that the apparent nonlinear density dependence, as well as the differences between DPB and HMS reported in experiment, largely rest on the behavior of the few highest density experimental points. The experimental rotation times of HMS and DPB are in fact the same to within the stated uncertainties, except at densities higher than $1.5\rho_c$. That Anderton and Kauffman chose to focus on the differences in the rotational behavior of these two solutes, rather than their similarities, largely rests on their adoption of the quasi-hydrodynamic model of Dote, Kivelson, and Schwartz[47] to interpret the experimental data. Using estimates for the free rotor times of 3.7 ps for DPB and 2.9 ps for HMS, such fits indicated an absence of density augmentation for the DPB/CO_2 system and ~40% density augmentation (at all densities) for HMS. Since these two solutes do rotate differently in hydrogen bonding solvents such as alcohols,[35] they reasonably attributed the difference observed in CO_2 to the ability of HMS to hydrogen bond to CO_2. However, the simulation data suggest a different perspective. First, the free rotor times used in their analysis are seen to substantially overestimate the true free rotor times of these solutes. As noted by Anderton and Kauffman,[19,43] within their modeling scheme, changes in these times have a dramatic impact on the extent of density augmentation deduced from rotation times. If the values of the free rotor times determined here (2.1 ps for DPB and 1.9 ps for HMS) were employed, significant and comparable density augmentation in the DPB/CO_2 and HMS/CO_2 systems would be implied by their analysis. Such an analysis would render the picture provided by the rotational measurements more in line with what we have deduced from spectral shift measurements. It would also largely obviate the need to invoke an important role for hydrogen bonding in the HMS/CO_2 system, which is not supported by the present calculations.

In summary, the rotation times obtained from these simulations are not in complete agreement with the experimental times measured by Anderton and Kauffman.[19] In addition to differences of interpretation, there does seem to be a systematic discrepancy between the simulated and observed times in the DPB/CO_2 system. We have suggested one possible experimental source for this discrepancy, but it must be admitted that the discrepancy could just as well reflect some shortcoming of the simulations. For example, it may be that the torsional flexibility of these solutes, which is not included in the simulations, might modify the rotational dynamics in some unknown way.[91] Only with further study on both fronts will we be able to discern the real cause for the disagreement. For now, we note that even if the present simulation models must ultimately be modified to

Solvation and Friction in Supercritical Fluids

J. Phys. Chem. B, Vol. 106, No. 28, 2002 **7107**

TABLE 4: Simulated Dynamical Properties[a]

density/ρ_c	$\tau_x^{(1)}$ /ps	$\tau_y^{(1)}$ /ps	$\tau_z^{(1)}$ /ps	$\tau_x^{(2)}$ /ps	$\tau_y^{(2)}$ /ps	$\tau_z^{(2)}$ /ps	D_{tr} /Å² ps⁻¹	$\tau_{\omega x}$ /ps	$\tau_{\omega y}$ /ps	$\tau_{\omega z}$ /ps	τ_v /ps	$\zeta_{\omega x}(0)$ /ps⁻²	$\zeta_{\omega y}(0)$ /ps⁻²	$\zeta_{\omega z}(0)$ /ps⁻²	$\zeta_{tr}(0)$ /ps⁻²
							DPB solute								
0.00	3.4	1.2	1.2	2.1	0.78	0.78									
0.25	5.6	2.8	2.7	2.9	1.3	1.5	5.4	0.32	0.93	1.6	4.8	63	43	15	24
0.47	8.4	4.2	5.1	3.7	2.0	2.1	2.6	0.16	0.53	1.0	2.4	103	72	26	40
0.63	10	5.1	5.6	4.1	2.0	2.5	1.8	0.14	0.42	0.93	1.7	120	85	33	46
0.80	12	5.6	5.9	4.3	2.2	2.4	1.3	0.12	0.41	0.80	1.1	130	91	34	50
1.05	16	6.3	6.8	6.1	2.9	2.9	1.2	0.086	0.34	0.57	0.95	158	113	46	61
1.48	19	8.4	9.1	7.1	3.4	4.1	0.88	0.075	0.23	0.42	0.69	188	137	58	75
1.69	25	10	11	9.1	4.0	4.9	0.69	0.055	0.20	0.36	0.60	209	148	64	82
1.90	27	12	13	9.3	4.4	5.2	0.58	0.056	0.17	0.35	0.44	231	166	73	91
2.00	29	11	13	9.7	4.6	5.6	0.56	0.047	0.15	0.32	0.45	252	181	79	100
							HMS solute								
0.00	3.2	1.2	1.2	2.0	0.79	0.79									
0.25	4.1	3.2	4.1	2.8	1.5	1.7	5.0	0.26	0.82	1.6	4.7	74	49	20	28
0.63	11	5.1	4.8	4.0	2.0	2.3	1.8	0.13	0.42	0.76	1.5	130	92	40	52
1.05	13	6.5	8.0	5.4	2.8	2.9	1.1	0.084	0.27	0.43	0.90	170	121	55	67
1.70	22	10	10	8.3	3.8	4.5	0.67	0.071	0.20	0.32	0.54	221	162	75	87
2.01	33	14	13	11	4.8	5.1	0.38	0.048	0.16	0.23	0.37	260	187	90	105

[a] $\tau_i^{(L)}$ are the correlation times of the L-th rank orientational correlation functions of principal axis i of the solute (eq 11) The values listed for $\rho = 0$ are the $1/e$ times of the free-rotor correlation functions. D_{tr} is the translational diffusion constant of the solute (eq 10), $\tau_{\omega i}$ and τ_v are the correlation times of the autocorrelation functions of the angular velocity about principal axis i and of the solute center-of-mass velocity (eqs 13,14), and $\zeta_{\omega i}(0)$ and $\zeta_{tr}(0)$ are the zero-time values of the orientational and translational friction functions, determined from the torques and forces on the solute according to eqs 17 and 19. $\tau_i^{(L)}$ times were determined by a combination of integration (to 50 ps) and exponential fitting. Uncertainties in these values (estimated as the standard error of the mean of 10−400 runs) are approximately ±10%. Uncertainties in D_{tr} are approximately ±15%. $\tau_{\omega i}$ values were obtained by direct integration (0−10 ps; ±8%). τ_v values were obtained by integration to 20 ps. In the case of the lowest densities (<0.5ρ_c) the integral of long-range tail, assumed to decay as $t^{-3/2}$, was also added (uncertainties are ±15%). Uncertainties in $\zeta_{\omega i}(0)$ and $\zeta_{tr}(0)$ are expected to be less than ±2%.

accurately reproduce the experimental rotation times, they are still more realistic than models used in most past simulations of supercritical solvation. It is therefore of interest to examine the simulated data further for what they might reveal about the nature of rotational dynamics and solvent friction in supercritical solvents, which is the topic of the final section of this paper.

D. Dynamics: The Density Dependence of Solvent Friction. In considering the density dependence of solvent friction we will only discuss results obtained with the DPB solute, simply noting that the conclusions we draw apply equally well to HMS. The basic quantities relevant to the rotational and translational dynamics of both systems are collected in Table 4.

Figure 14 summarizes the orientational correlation times and translational diffusion constants observed in the DPB/CO₂ system. The panels labeled "$L = 1$" and "$L = 2$" are the correlation times $\tau_i^{(L)}$ of the 1st and 2nd rank functions $C_i^{(L)}(t)$ (eq 11) for all three inertial axes, $i = x, y, z$. As already noted with respect to $\tau_x^{(2)}$, these correlation times are all approximately linear functions of density. The lines are fits to the nonzero density data, and the "+" symbols denote $1/e$ times of the free rotor correlation functions. These free rotor times are seen to provide reasonable estimates of the zero-density intercepts of the (integral) correlation times measured at finite densities. We note that although $1/e$ and integral times are identical in the case of exponential $C_i^{(L)}(t)$, they need not agree in general. In fact, the integral times of ($L = 2$) free rotor correlation functions are infinite in many cases, and are thus of little use in thinking about the behavior at finite densities. Nevertheless, we find that in the present simulations, and in calculations with the J-diffusion model[92] for rotors of various symmetries, such free rotor $1/e$ times provide a useful approximation for the zero-density intercepts of finite-density rotation times. This observation suggests that it is reasonable to regard the difference $\tau_i^{(L)}(\rho) - \tau_{i,fr}^{(L)}$ as a measure of solvent friction, as is often done in experiment.
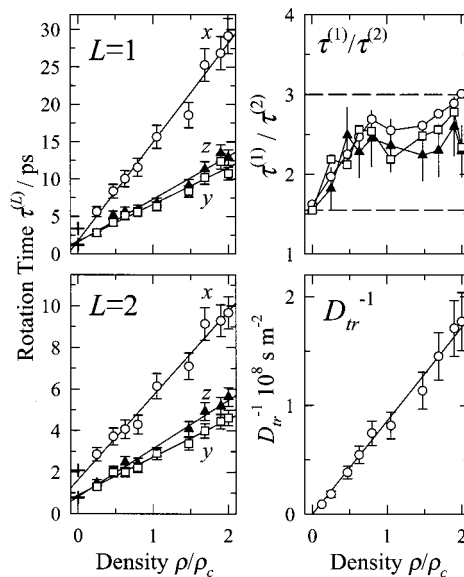

Figure 14. Orientational correlation times and translational diffusion constants of DPB as functions of CO₂ density. The panels labeled "$L = 1$" and "$L = 2$" are correlation times of the 1st and 2nd rank orientational correlation functions and the panel labeled "$\tau^{(1)}/\tau^{(2)}$" is the ratio of these times. Open circles, open squares, and filled triangles denote times of the x, y, and z principal axes, respectively. The "+" symbols indicate $1/e$ times of the free rotor correlation functions. (The x axis rotation shows the largest free rotor time; the times for the y and z axes are indistinguishable here.) The panel labeled "D_{tr}^{-1}" shows the inverse of the translational diffusion constants of DPB.

The panel labeled "$\tau^{(1)}/\tau^{(2)}$" in Figure 14 shows the ratio of 1st to 2nd rank rotation times, a ratio which is often taken as an indication of the relative importance of inertial versus diffusive behavior. The horizontal dashed lines in this panel indicate the limiting values predicted for low ($\tau^{(1)}/\tau^{(2)} \rightarrow 3\sqrt{3}/11$) and high ($\tau^{(1)}/\tau^{(2)} \rightarrow 3$) friction by a model designed

to treat spherical rotors.[93] These plots show that the low-friction limit of this spherical top model also predicts the free rotor behavior of an asymmetric solute such as DPB. In contrast, at high densities, the limiting value of 3 does not appear to be approached in all cases. Based on an analysis to be discussed shortly, we estimate that the x, y, and z axis ratios should approach limits of approximately 3.0, 2.6, and 2.4, respectively. These limiting values are nearly achieved at densities not much greater than $0.5\rho_c$. From this observation, we conclude that inertial motions have little impact on the rotational dynamics of this large solute beyond this relatively low supercritical density.

The final panel of Figure 14, labeled "D_{tr}^{-1}" shows the translational diffusion constants of the solute, calculated according to eq 10. Like the difference $\tau_i^{(L)}(\rho) - \tau_{i,fr}^{(L)}$, this inverse rate is expected to be directly proportional to solvent friction. As in the case of rotational friction, the translational friction appears to be simply proportional to solvent density. Given the presence of significant density augmentation which renders the local environment a nonlinear function of density, this linear behavior of the friction is puzzling. To understand this behavior, we must consider the nature of the time-dependent friction underlying the observable rotation times and diffusion constant.

An understanding of how fluctuating solvent forces lead to frictional damping of solute translation and rotation is best achieved through an examination of the respective velocities. The essential information is contained in the autocorrelation functions of the solute center of mass velocity $\vec{v}(t)$

$$C_v(t) = \frac{\langle \vec{v}(0) \cdot \vec{v}(t) \rangle}{\langle v^2 \rangle} \tag{13}$$

and the angular velocities $\omega_i(t)$ about the solute principal inertial axes $i = x, y, z$

$$C_{\omega i} = \frac{\langle \omega_i(0) \omega_i(t) \rangle}{\langle \omega_i^2 \rangle} \tag{14}$$

Representative velocity autocorrelation functions of DPB at several CO_2 densities are shown in Figure 15. In contrast to the behavior of the $C_i^{(L)}(t)$ these velocity correlation functions decay more rapidly as solvent density increases, a trend that primarily[94] reflects the more rapid loss of memory of directional motion as interactions with the solvent increase. The correlation times of these functions, which are listed in Table 4, can therefore be interpreted as effective collision times for the various types of motions. As can be seen from these data the rate at which solute−solvent interactions randomize rotational motion increases in the order $z < y < x$, a trend which reflects both the volume swept out by the solute and the inertial frequencies of these different rotations. (Because we only consider the total solute linear velocity, $C_v(t)$ contains motions similar to all three rotations and this correlation function contains both fast and slow components, as can be seen in Figure 15.)

Friction can be related to these velocity autocorrelation functions and then to observable rotation and diffusion times by considering generalized Langevin equations (GLEs) for $\vec{v}(t)$ and $\omega_i(t)$. The case of translational motion is simple and well-known, so we consider it first. The GLE defining the time-dependent translational friction function $\zeta_{tr}(t)$ is[95]

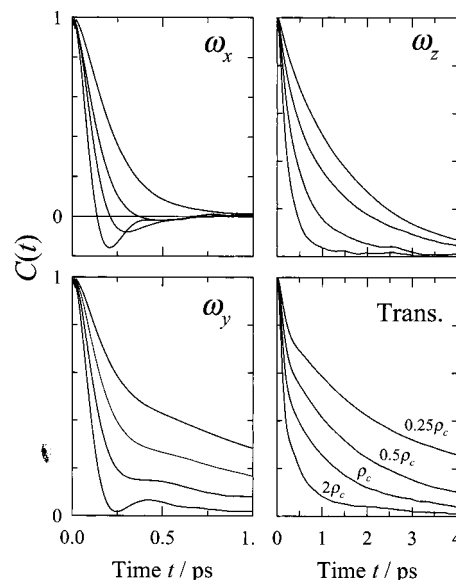$$m\frac{d\vec{v}}{dt} = -m\int_0^t d\tau \zeta_{tr}(t - \tau)\vec{v}(\tau) + \vec{F}_r(t) \tag{15}$$

Figure 15. Solute angular ("ω_i", $C_{\omega i}(t)$, eq 14) and center-of-mass ("trans", $C_v(t)$, eq 13) velocity autocorrelation functions of DPB at a series of CO_2 densities: 0.25, 0.47, 1.05, and $2.00\rho_c$. In all cases, increasing density increases the rate of decay of the correlation functions as indicated on the bottom right panel. The vertical scale on these plots runs from 0 to 1 with the exception of the ω_x plot, which begins at -0.2. (Note the difference in the horizontal scales used for the ω_x and ω_y versus the ω_z and "trans" plots.)

where m is the solute mass and $\vec{F}_r(t)$ the "random force" acting on the solute, which is related to $\zeta_{tr}(t)$ by

$$\zeta_{tr}(t) = \frac{\langle \vec{F}_r(0) \cdot \vec{F}_r(t) \rangle}{3mk_BT} \tag{16}$$

Equation 16 clearly exposes the fact that the fluctuating interactions with solvent molecules act on average to damp solute motions. This net frictional effect is summarized by the function $\zeta_{tr}(t)$ and its rotational counterpart, which are therefore the key quantities for describing the solvent's influence over solute motion. It should be noted that the random force in eq 16 is not directly available from simulated trajectories because the evolution of $\vec{F}_r(t)$ is governed not by the full system Liouville operator but rather by one in which the solute dynamics of interest have been projected out. (For a solute much more massive than the solvent, the dynamics of $\vec{F}_r(t)$ are similar to the forces that would be observed in a simulation of a stationary solute.[96]) However, $\zeta_{tr}(t)$ can be obtained from a knowledge of the velocity autocorrelation function because the two are related by the memory function equation[95]

$$\frac{dC_v}{dt} = -\int_0^t d\tau \zeta_{tr}(t - \tau)C_v(\tau) \tag{17}$$

Given $C_v(t)$ data of the sort shown in Figure 14, $\zeta_{tr}(t)$ can be obtained by inversion of this integral equation.[97]

Determining the time-dependent friction relevant for rotation of an asymmetric solute like DPB is more complicated than in the case of translation just described. What is simple, and strictly analogous to the translational case is the rotation of a rigid linear solute. Here, one can write a rigorous generalized Langevin equation for the angular velocity $\vec{\omega}(t)$ of the solute with moment of inertia I as[98]

Solvation and Friction in Supercritical Fluids

J. Phys. Chem. B, Vol. 106, No. 28, 2002 **7109**

$$I\frac{d\vec{\omega}}{dt} = -I\int_0^t d\tau \zeta_\omega(t-\tau)\vec{\omega}(\tau) + \vec{T}_r(t)$$

$$\zeta_\omega(t) = \frac{\langle\vec{T}_r(0)\cdot\vec{T}_r(t)\rangle}{2Ik_BT} \quad (18)$$

where $\zeta_{rot}(t)$ is the rotational friction kernel and $\vec{T}_r(t)$ the random torque due to solvent interactions. For an asymmetric solute, however, there is no completely rigorous equivalent to eq 18.[99] We therefore adopt a phenomenological description of the rotational motion and *define* the effective rotational friction acting on each principal coordinate axis i by the memory function equation for $C_{\omega i}(t)$

$$\frac{dC_{\omega i}}{dt} = -\int_0^t d\tau \zeta_{\omega i}(t-\tau)C_{\omega i}(\tau) \quad (19)$$

Such $\zeta_{\omega i}(t)$ functions can be viewed as being related to the random torques acting on each axis i, via the approximate GLE equations

$$I_i\frac{d\omega_i}{dt} \cong -I_i\int_0^t d\tau \zeta_{\omega i}(t-\tau)\omega_i(\tau) + T_{ri}(t)$$

$$\zeta_{\omega i}(t) = \frac{\langle T_{ri}(0)T_{ri}(t)\rangle}{I_ik_BT} \quad (20)$$

where ω_i is the body-fixed angular velocity component and I_i the corresponding moment of inertia about axis i. Equation 20 is not exact because it neglects cross terms in $\omega_i(t)\omega_j(t)$ which arise due to the nonseparability of angular coordinates. It also assumes that the principal axes of inertia and diffusion coincide. However, neither of these approximations is especially damaging for the large, nearly symmetric molecules examined here and the friction functions defined by eq 20 provide a useful representation of the rotational motion in the present systems.

To demonstrate the utility of the rotational friction functions so defined, we digress to consider how they relate to the reorientational correlation functions $C_i^{(L)}(t)$ in the diffusive limit. In this limit the time-dependence of $\zeta_{\omega i}(t)$ is unimportant, what matters are the integral friction constants $\zeta_{\omega i}$, related to the rotational diffusion constants D_i by[100-102]

$$D_i = \frac{k_BT}{I_i\zeta_{\omega i}} \quad (21)$$

(The friction constants are obtained from angular velocity autocorrelation times as discussed below.) Reorientation motion of a principal axis i can be described in this limit by

$$C_i^{(1)}(t) = \exp\{-(3D_{rot}-D_i)t\} \quad (22)$$

$$C_i^{(2)}(t) = \left(\frac{1}{2}+\frac{3(D_{rot}-D_i)}{4\Delta}\right)\exp\{-(6D_{rot}+2\Delta)t\} + \left(\frac{1}{2}-\frac{3(D_{rot}-D_i)}{4\Delta}\right)\exp\{-(6D_{rot}-2\Delta)t\} \quad (23)$$

where

$$D_{rot} = \frac{1}{3}(D_x+D_y+D_z) \text{ and}$$

$$\Delta = \sqrt{D_x^2+D_y^2+D_z^2-D_xD_y-D_xD_z-D_yD_z} \quad (24)$$

Figures 16 and 17 illustrate the extent to which such a description represents the rotational dynamics actually observed.
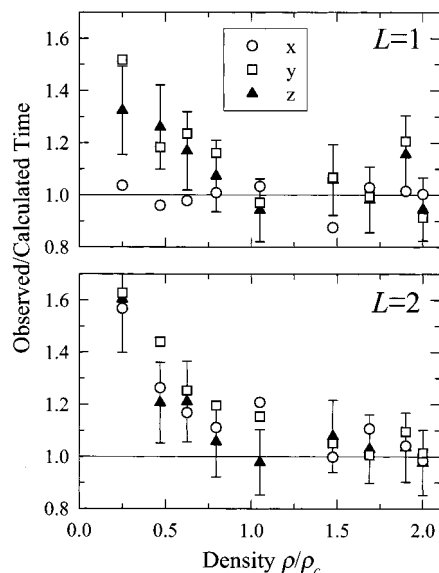

Figure 16. Ratios of observed reorientational correlation times $\tau_i^{(L)}$ to times calculated using the rotational diffusion constants defined by eq 21 and the diffusive-limit prediction, eq 23. Open circles, open squares, and filled triangles represent $i = x$, y, and z, respectively. (For clarity, uncertainties are indicated only for the $\tau_z^{(L)}$ points.)
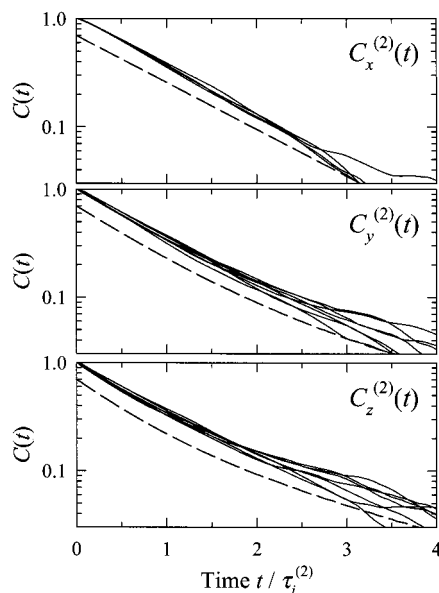

Figure 17. Observed (solid curves) reorientational correlation functions $C_i^{(2)}(t)$ compared to those calculated for the diffusive-limit (dashed curves) according to eq 23. To focus on the shapes of these curves, in each case the time axis has been scaled by the respective value of the correlation time $\tau_i^{(2)}$. Simulation data are shown for densities of $0.63-2.0\rho_c$ in the case of $i = y$ and z and $1.0-2.0\ \rho_c$ in the case of $i = x$. Curves calculated from eq 23 vary insignificantly with density. The curves shown, which are vertically shifted for clarity, correspond to the functions: $C(t) = f_1\exp(-t/\tau_1) + (1-f_1)\exp(-t/\tau_2)$ with the following constants: (x: $f_1 = 0.99$, $\tau_1^* = 1.01$, $\tau_2^* = 0.36$), (y: $f_1 = 0.83$, $\tau_1^* = 0.76$, $\tau_2^* = 2.15$), and (z: $f_1 = 0.66$, $\tau_1^* = 0.62$, $\tau_2^* = 1.75$) where "*" indicates normalization by the correlation time.

In Figure 16, we plot the ratios of the correlation times $\tau_i^{(L)}$ observed to those calculated using eqs 21−24. The observed correlation times tend to be larger than the calculated ones. But, down to a density of $0.5\rho_c$ the difference is small, less than $\sim20\%$. This observation supports the conclusion that rotations of DPB are essentially diffusive in character beyond $\rho = 0.5\rho_c$. In addition, the time-dependence of the correlation functions,
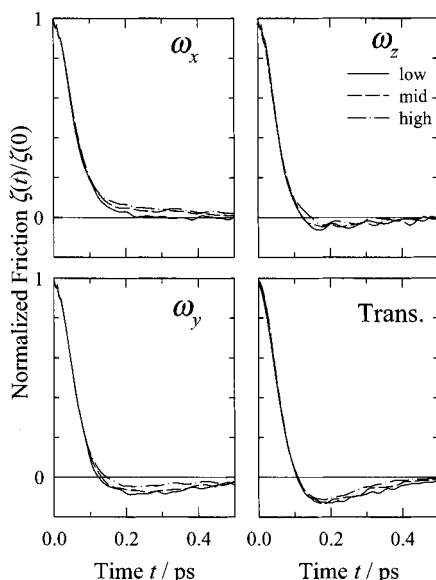
Figure 18. Normalized time-dependent friction functions $\zeta(t)/\zeta(t = 0)$ determine by inverting the memory function equations of the respective velocity autocorrelation functions (eqs 17 and 19.) To average some of the noise in these functions and make the density dependence clearer, each of the curves depicted here has been averaged over three densities: "low" (solid curve) are the lowest three densities, "mid" (dashed) the three middle, and "high" (dash−dot) the three highest densities simulated.

depicted in Figure 17, is also reasonably reproduced by these diffusive-limit calculations for $\rho > 0.5\rho_c$. To within the uncertainties in the data, except near $t = 0$, all of the $L = 1$ correlation functions (not shown) as well as $C_x^{(2)}(t)$ can be represented as single-exponential functions of time, in accordance with eqs 22 and 23. In the case of $C_y^{(2)}(t)$ and $C_z^{(2)}(t)$, where eq 23 predicts a biexponential decay with a shape that is virtually density independent, Figure 17 shows that the observed correlation functions display a nonexponential character that appears to follow these predictions to within the uncertainties in the data. For densities $\leq 0.5\rho_c$ both the times and the shapes of the correlation functions depart significantly from these predictions. This departure comes from two sources: (i) the inaccuracy associated with using a diffusive description of the motion, i.e., the error incurred by neglecting the time-dependence of $\zeta_{\omega i}(t)$ at low densities, and (ii) the inaccuracy in using $\zeta_{\omega i}(t)$ defined by eq 19 and the approximate GLE of eq 20 as a description of the rotational motion. Although we do not know how to disentangle these two effects, we adopt the viewpoint that much of the deviation can be ascribed to the first effect. We therefore conclude that, despite the difficulties in formulating a rigorous GLE description of the rotational motion of an arbitrary asymmetric molecule, the effective friction defined by eq 19 is a good working substitute − if not at all densities, at least down to densities of on the order of $0.5\rho_c$ in the present systems. In what follows we will simply refer to $\zeta_{\omega i}(t)$ as the time-dependent rotational friction.

Having clarified our definition of rotational friction in these systems, we return to examining the dependence of friction on density. Rotational and translational friction functions obtained through inversion of velocity autocorrelation function data[97] are shown in normalized form in Figure 18. Due to the numerical difficulties inherent in inverting memory function equations (eqs 17 & 19), the $\zeta_{\omega i}(t)$ and $\zeta_{tr}(t)$ functions are noisy, and for this reason, we display results averaged into low-, mid-, and high-density curves. In marked contrast to the orientational and

angular velocity correlation functions, the time dependence of these friction functions is nearly independent of density. The short time dynamics are quite similar for all four functions, consisting of an approximately Gaussian decay with a half width of ~50 fs in all cases ($\omega_x = 57$, $\omega_y = 54$, $\omega_z = 49$, and Trans $= 49 \pm 1$ fs). This rapid initial decay reflects the fast force fluctuations that result from repulsive interactions with solvent molecules.[103] The fact that this part of the dynamics is virtually independent of solvent density implies that such repulsive interactions can be treated as independent binary (i.e., solute − single-solvent) events. The tails of the various friction functions, however, do differ noticeably from one another, and they also vary systematically with solvent density. In all cases, the tails of $\zeta(t)$ decay on the time scale of a few hundred femtoseconds and their amplitudes become more positive with increasing solvent density. This latter component of the friction reflects slower fluctuations in the forces acting on the solute, fluctuations which are primarily due to attractive solute−solvent interactions. The fact that there is a systematic change with density signals the importance of solvent−solvent correlations in this slower component of the friction.[103]

Of course, the normalized functions $\zeta(t)/\zeta(t = 0)$ of Figure 18 show only a part of the dependence of friction on density. Much more important to the observed variations in rotation times and diffusion rates are changes in the amplitudes $\zeta(t = 0)$ of these functions with density. Since a diffusive description is adequate at most densities, we can ignore the detailed time-dependence of $\zeta(t)$ and consider the observed translational and rotational dynamics to result from the integral friction, the product of $\zeta(t = 0)$ and the correlation times, τ_ζ, of these functions. Working in this limit is convenient because one does not need to perform the (noisy) inversion of eqs 17 and 19 in order to obtain these two characteristics of the friction. The time-zero amplitude of $\zeta(t)$ can be determined from the forces and torques observed in simulation using eqs 16 and 20 (because there is no distinction between the "random" and actual forces at $t = 0$):

$$\zeta_{tr}(t = 0) = \frac{\langle|\vec{F}|^2\rangle}{3mk_BT} \text{ and } \zeta_{\omega i}(t = 0) = \frac{\langle T_i^2\rangle}{I_i k_B T} \quad (25)$$

In addition, Laplace transformation of the memory function equation shows that the integral friction is equal to the inverse of the correlation time of the appropriate velocity autocorrelation function[95]

$$\zeta_{tr} \equiv \int_0^\infty \zeta_{tr}(t)dt = \left\{\int_0^\infty C_v(t)dt\right\}^{-1} \equiv \tau_v^{-1} \quad \left(= \frac{k_B T}{m D_{tr}}\right) \quad (26)$$

and

$$\zeta_{\omega i} \equiv \int_0^\infty \zeta_{\omega i}(t)dt = \left\{\int_0^\infty C_{\omega i}(t)dt\right\}^{-1} \equiv \tau_{\omega i}^{-1} \quad \left(= \frac{k_B T}{I_i D_i}\right) \quad (27)$$

The correlation times of the friction functions can therefore be obtained via the relation $\tau_\zeta = \zeta/\zeta(t = 0)$, without knowledge of the detailed time dependence of $\zeta(t)$. Friction characteristics determined in this manner are plotted versus density in Figure 19.

The upper left panel of Figure 19 shows the various integral friction constants together with fits to $\zeta = \text{const} \times \rho$. As would be anticipated from the linear behavior of the reorientation times and translational diffusion constant with density (Figure 14), the friction constants are approximately proportional to density.
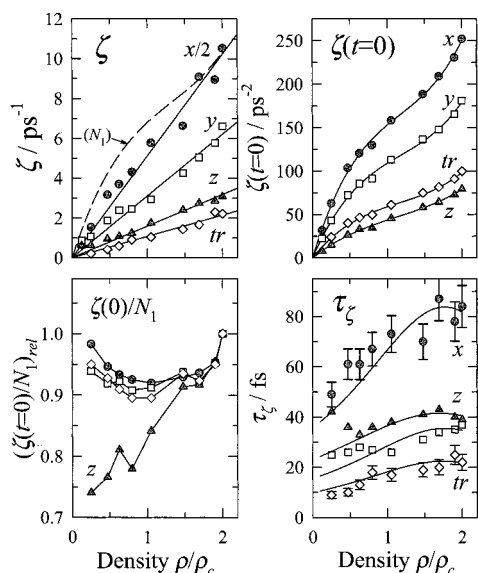
Solvation and Friction in Supercritical Fluids

J. Phys. Chem. B, Vol. 106, No. 28, 2002 **7111**

Figure 19. Density dependence of the integral friction ζ and its decomposition into amplitude $\zeta(t = 0)$ and correlation time τ_ζ contributions. In all cases filled circles denote friction on ω_x, open squares ω_y, filled triangles ω_z, and open diamonds on translational motion. The panel labeled "ζ" contains the integral friction constants. The values of $\zeta_{\omega x}$ have been reduced by a factor of 2 for display purposes. The solid lines in this panel are fits to a proportionality, $\zeta = \text{const} \times \rho$. The dashed line is a fitted and scaled representation of the dependence of the 1st coordination number on density, $N_1(\rho)$. The panel labeled "$\zeta(t = 0)$" are the time-zero amplitudes of the friction functions. The curves shown here are cubic fits used to highlight the density dependence. The panel labeled "$\zeta(0)/N_1$" shows these time-zero amplitudes ratioed to the 1st shell coordination number and also normalized to the value of $\zeta(0)/N_1$ at the highest density $2\rho_c$. The plot labeled τ_ζ shows the correlation times (points), determined from $\tau_\zeta = \zeta/\zeta(t = 0)$. The solid curves in this panel show the dependence of τ_ζ-(ρ) calculated via this equation, using as input the smoothed density dependence of ζ (straight lines) and $\zeta(t = 0)$ (smooth curves) shown in their respective panels.

(The one exception is $\zeta_{\omega z}$, which does not decrease sufficiently near to $\rho=0$ to maintain this proportionality.) As noted earlier, finding the net friction to be simply proportional to density is puzzling since it suggests, at least superficially, that the friction is ignorant of the substantial density augmentation present in the DPB/CO_2 system. The extent of the density augmentation is represented in this panel by the dashed line labeled "(N_1)", which shows a scaled version of the (fitted) density dependence of the 1st solvation shell coordination number. However, dissection of the integral friction into its amplitude and temporal components (the other panels in Figure 19) shows how this behavior arises. In the panel labeled "$\zeta(t=0)$" are the frictional amplitudes. Unlike the integral friction, these time-zero amplitudes are clearly nonlinear functions of density. The shapes of these curves are similar to that of $N_1(\rho)$. This similarity is quantified in the panel labeled "$\zeta(0)/N_1$", where we have plotted the ratio of the time-zero amplitudes to the 1st shell coordination numbers. (The values plotted here have all been normalized to their respective values at $\rho = 2\rho_c$.) From this representation of the data, it is clear that the *amplitude* of the friction *is* sensitive to density augmentation. With the exception of the friction on ω_z, the ratios $\zeta(0)/N_1$ vary by only $\pm5\%$ over the density range studied. In these cases, $\zeta(t = 0)$ is tracking the local density quite closely. Given that the amplitude of the friction is dominated by repulsive solute−solvent interactions, together with the facts that such dynamics are largely independent and are negligibly small for solvent molecules not in the 1st solvation

shell, this close correspondence is understandable. The fact that $\zeta_{\omega z}(0)$ fails to track N_1 as faithfully as the other functions is likely to be the result of the asymmetry in the density buildup around the solute (Figure 4). Rotation about the (out-of plane) z inertial axis is mainly affected by interactions with solvent molecules around the periphery of the molecular plane. Because the relative enhancement of solvent density in this region is much smaller than above and below the molecular plane at low densities, a reduced friction relative to the other motions is to be expected.

Finally, the panel labeled "τ_ζ " in Figure 19 shows how the correlation times of the various friction functions depend on density. Although these data (points) are noisy, with the exception of $\tau_{\omega z}$, the trend is for the memory relaxation times to increase with increasing density. Because the initial dynamics of $\zeta(t)$ change negligibly with density, this increase must result from the rather subtle changes in the "long-time" tails of the friction functions shown in Figure 18. These variations in the tails of the friction functions, which we attribute to changes in the collective nature of attractive solute−solvent interactions, are responsible for obscuring the obvious curvature in the time-zero friction values and the apparently linear behavior of the integral friction with density. (To illustrate how the density dependence of these times can negate the curvature in $\zeta(t = 0)$, the smooth curves in this panel display the $\tau_\zeta(\rho)$ dependence required to transform the fitted values of $\zeta(t = 0)$ into the simple proportionalities (lines) shown in panel "ζ".) Thus, it is not that the rotational and translational dynamics are ignorant of the density augmentation. Rather, it is a curious cancellation between the short-time (repulsive) and long-time (attractive) components of the friction that gives rise to this apparent insensitivity to local density. We note that very similar behavior was also observed in recent simulations of translational diffusion in Lennard−Jones systems by Yamaguchi et al.[15]

V. Summary & Conclusions

In the present study, we have used computer simulations of two diphenyl polyenes in supercritical CO_2 to explore the connections between local density augmentation and solute friction. We have employed what we believe to be realistic models of these systems in an attempt to accurately reproduce experimental observations and provide molecular-level insights into these systems. We have been at least partially successful in this endeavor. The extent of the density augmentation deduced from measurements of electronic spectral shifts is reasonably captured by the present simulations. Simulated values are slightly smaller than those derived from experiment, with the differences being close to experimental uncertainties. The difference would not be noteworthy except that it is consistent with a general discrepancy between simulation and experiment previously uncovered in a survey of available augmentation data.[10] The origins of this discrepancy are not known with certainty, but we believe that it mainly reflects inaccuracies in the modeling of electronic spectral shifts. Support for such an interpretation comes from recent observations made by Fernandez-Prini and co-workers in integral equation studies, who noted that systematically different interaction parameters are required to model thermodynamic versus spectroscopic properties of solutes in supercritical solvents.[104,105] These interesting observations aside, the agreement between simulated and experimental measures of density augmentation is sufficient to warrant the conclusion that the representation of solvation structure in these simulations is fairly realistic.

The situation is less satisfying when it comes to modeling solute rotational dynamics. Despite the fact that two measures

of solvent friction, the solvent viscosity and self-diffusion coefficient, are nicely reproduced by the simulations, the simulated rotational behavior of DPB and HMS is not in good agreement with the experimental results of Anderton and Kauffman.[19] The large differences in rotation times measured for DPB and HMS are not reproduced in the simulations. Consistent with this lack of solute dependence, the simulations do not find HMS−CO_2 hydrogen bonding to be a significant influence on either augmentation or rotational dynamics in these systems, contrary to what was inferred from the rotation data. The primary source of the disagreement between the simulation and these experiments lies in the rotation times of DPB at higher densities, where the simulated times are roughly 30% greater than the measured values. Whether this discrepancy results from inaccurate or incomplete simulation models or to inaccuracies in the experimental data or its analysis must await further study. We hope to undertake such work in the future, extending the experiments to measurements of time-resolved anisotropies and the simulations to include flexible models of the solute in order to examine isomerization reactions of these solutes.

Even if the current potential models are not completely faithful representations of the experimental systems, two general lessons can still be learned from the dynamics simulated here. First, the simulations indicate that it is reasonable to use the difference between observed rotation times and free rotor times to measure the extent of friction in supercritical solvents. This practice, which was employed by Anderton and Kauffman,[19] is preferable to comparing observed rotation times directly to frictional models at low densities (as was done in previous work by our group[17]). One should, of course, use appropriate values for the free rotor times for performing such subtractions. The present results, together with model calculations on a variety of rotor symmetries, show that rotation times often extrapolate to the 1/e times of free rotor correlation functions, and that these times are represented accurately in most cases by $\tau_{fr}^{(2)} \cong 0.83 \sqrt{I_{eff}/k_B T}$, where I_{eff} is the harmonic mean of the two inertial moments that rotate the solute axis being observed.[106]

The second lesson is that the way in which local density augmentation affects solute dynamics may be rather subtle. In the cases studied here (both DPB and HMS), the net friction constants controlling rotational and translational motion were found to be approximately proportional to bulk solvent density, i.e., apparently ignorant of the considerable density augmentation present in these systems. This ignorance is only apparent, however, in that it results from a curious cancellation of opposing tendencies. Whereas the average forces and torques on the solute (i.e., the friction amplitude $\zeta(0)$) faithfully mirror local densities, the correlation times of these (random) forces, i.e., the correlation times of $\zeta(t)$, change with density in such a way that the net friction lacks any clear signature of density augmentation. Because quite similar observations were made by Yamaguchi et al.[15] in simulations of translational diffusion of Lennard−Jones solutes, it may be that this apparent failure of diffusive motions to report on local density is a general feature of supercritical solvation.[107] It results from the evolution of the "long-time" tails of the friction with density, which, at super-critical densities, is probably mainly associated with fluctuations in attractive solute−solvent forces. Further simulation studies, and more sophisticated analytic theories than are currently available will be required to fully understand this curious behavior.

Supporting Information Available: Summary of all of the potential parameters as well as the solute geometries used in these simulations, transition monopole values derived from AM1/CI calculations[75], DPB and HMS frequencies in 20 liquid solvents and in the gas phase, and a complete listing of charge distributions in DPB and HMS. This material is available free of charge via the Internet at http://pubs.acs.org.

References and Notes

(1) The special issue of Chemical Reviews, Vol. 99, Issue 2, edited by R. Noyori, as well as refs 2−6 provide useful introductions to recent activity in this area.

(2) *Chemical Synthesis using Supercritical Fluids*; Jessop, P. G., Leitner, W., Eds.; Wiley-VCH: New York, 1999.

(3) McClain, J. B. *Chem. Eng.* **2000**, 72.

(4) Eckert, C. A.; Knutson, B. L.; Debenedetti, P. G. *Nature* **1996**, *383*, 313.

(5) Phelps, C. L.; Smart, N. G.; Wai, C. M. *J. Chem. Edu.* **1996**, *73*, 1163.

(6) Kajimoto, O. *Chem. Rev.* **1999**, *99*, 355.

(7) Brennecke, J. F.; Chateauneuf, J. E. *Chem. Rev.* **1999**, *99*, 433.

(8) Tucker, S. C. *Chem. Rev.* **1999**, *99*, 391.

(9) Lewis, J.; Biswas, R.; Robinson, A.; Maroncelli, M. *J. Phys. Chem. B* **2001**, *105*, 3306.

(10) Song, W.; Biswas, R.; Maroncelli, M. *J. Phys. Chem. A* **2000**, *104*, 6924.

(11) Egorov, S. *J. Chem. Phys.* **2000**, *112*, 7138.

(12) Yamaguchi, T.; Kimura, Y.; Hirota, N. *J. Chem. Phys.* **1999**, *111*, 4169.

(13) Drozdov, A. N.; Tucker, S. *J. Phys. Chem. B* **2001**, *105*, 6675.

(14) Itoh, K.; Holroyd, R.; Nishikawa, M. *J. Phys. Chem. A* **2001**, *105*, 703.

(15) Yamaguchi, T.; Kimura, Y.; Hirota, N. *Mol. Phys.* **1998**, *94*, 527.

(16) Higashi, S.; Iwai, Y.; Takahashi, Y.; Uchida, H.; Arai, Y. *Fluid Phase Equilibria* **1998**, *144*, 269.

(17) Heitz, M. P.; Maroncelli, M. *J. Phys. Chem. A* **1997**, *101*, 5852.

(18) Heitz, M. P.; Bright, F. V. *J. Phys. Chem.* **1996**, *100*, 6889.

(19) Anderton, R. M.; Kauffman, J. F. *J. Phys. Chem.* **1995**, *99*, 13 759.

(20) Vikhrenko, V. S.; Schwarzer, D.; Schroeder, J. *Phs. Chem. Chem. Phys.* **2001**, *3*, 1000.

(21) Schwarzer, D.; Troe, J.; Zerezke, M. *J. Chem. Phys.* **1997**, *107*, 8380.

(22) Yamaguchi, T.; Hirota, N. Vibrational Energy Relaxation of Azulene in the S_2 State. II. Solvent Density Dependence. In. *J. Chem. Phys.* **2000**, *113*, 4340.

(23) Myers, D. J.; Shigeiwa, M.; Fayer, M. D.; Cherayil, B. J. *J. Phys. Chem. B* **2000**, *104*, 2402.

(24) Frankland, S. J. V.; Maroncelli, M. *J. Chem. Phys.* **1999**, *110*, 1687.

(25) Pan, X.; McDonald, J. C.; MacPhail, R. A. *J. Chem. Phys.* **1999**, *110*, 1677.

(26) Tucker, S. C.; Maddox, M. W. *J. Phys. Chem. B* **1998**, *102*, 2437.

(27) Egorov, S.; Rabani, E. *J. Chem. Phys.* **2002**, *116*, 8447.

(28) Egorov, S.; Rabani, E. *J. Chem. Phys.* **2001**, *115*, 617.

(29) Zhang, J.; Roek, D. P.; Chateauneuf, J. E.; Brennecke, J. F. *J. Am. Chem. Soc.* **1997**, *119*, 9980.

(30) Ganapathy, S.; Carlier, C.; Randolph, T. W.; O'Brien, J. A. *Ind. Eng. Chem. Res.* **1996**, *35*, 19.

(31) Kimura, Y.; Yoshimura, Y. *J. Chem. Phys.* **1992**, *96*, 3085.

(32) Drozdov, A. N.; Tucker, S. *J. Chem. Phys.* **2001**, *114*, 4912.

(33) deGrazia, J. L.; Randolph, T. W.; O'Brien, J. A. *J. Phys. Chem. A* **1998**, *102*, 1674.

(34) Anderton, R. M.; Kauffman, J. F. *J. Phys. Chem.* **1994**, *98*, 12 117.

(35) Wiemers, K.; Kauffman, J. F. *J. Phys. Chem. A* **2000**, *104*, 451.

(36) We have also recently examined the rotational dynamics of DPB in liquid alkane and perfluoroalkane solvents (K. Dahl, R. Biswas, and M. Maroncelli, manuscript in preparation) and Schroeder and co-workers have examined DPB in low-density alkane solvents.[112]

(37) Wiemers, K.; Kauffman, J. F. *J. Phys. Chem. A* **2001**, *105*, 823.

(38) Anderton, R. M.; Kauffman, J. F. *J. Phys. Chem.* **1994**, *98*, 12 125.

(39) Mohrschladt, R.; Schroeder, J.; Schwarzer, D.; Troe, J.; Vohringer, P. *J. Chem. Phys.* **1994**, *101*, 7566.

(40) Gehrke, C.; Mohrschladt, R.; Schroeder, J.; Troe, J.; Vohringer, P. *Chem. Phys.* **1991**, *152*, 45.

Solvation and Friction in Supercritical Fluids

J. Phys. Chem. B, Vol. 106, No. 28, 2002 **7113**

(41) Velsko, S. P.; Fleming, G. R. *J. Chem. Phys.* **1982**, *76*, 3553.

(42) Kauffman, J. F. *J. Phys. Chem. A* **2001**, *105*, 3433.

(43) Kauffman, J.; Wiemers, K.; Khajehpour, M. *Rev. High-Pressure Sci. Technol.* **1998**, *7*, 1225.

(44) Gehrke, C.; Schroeder, J.; Schwarzer, D.; Troe, J.; Voss, F. *J. Chem. Phys.* **1990**, *92*, 4805.

(45) Courtney, S. H.; Fleming, G. R. *Chem. Phys. Lett.* **1984**, *103*, 443.

(46) Lakowicz, J. R. *Principles of Fluorescence Spectroscopy*, 2nd ed.; Plenum Press: New York, 1999.

(47) Dote, J. L.; Kivelson, D.; Schwartz, R. N. *J. Phys. Chem.* **1981**, *85*, 2169.

(48) Singh, M. *Photochem. Photobiol.* **2000**, *72*, 438.

(49) De Backer, S.; Dutt, G. B.; Ameloot, M.; De Schryver, F. C.; Mullen, K.; Holtrup, F. *J. Phys. Chem.* **1996**, *100*, 512.

(50) Roy, M.; Doraiswamy, S. *J. Chem. Phys.* **1993**, *98*, 3213.

(51) Horng, M.-L.; Gardecki, J.; Maroncelli, M. *J. Phys. Chem.* **1997**, *101*, 1030.

(52) See, for example, the discussion in footnote 77 of ref 17.

(53) Harris, J. G.; Yung, K. H. *J. Phys. Chem.* **1995**, *99*, 12 021.

(54) Jorgensen, W. L. BOSS, Version 4.2, Yale University, 2000.

(55) Frisch, M. J.; Trucks, G. W.; Schlegel, H. B.; Scuseria, G. E.; Robb, M. A.; Cheeseman, J. R.; Zakrzewski, V. G.; Montgomery, J. A., Jr.; Stratmann, R. E.; Burant, J. C.; Dapprich, S.; Millam, J. M.; Daniels, A. D.; Kudin, K. N.; Strain, M. C.; Farkas, O.; Tomasi, J.; Barone, V.; Cossi, M.; Cammi, R.; Mennucci, B.; Pomelli, C.; Adamo, C.; Clifford, S.; Ochterski, J.; Petersson, G. A.; Ayala, P. Y.; Cui, Q.; Morokuma, K.; Malick, D. K.; Rabuck, A. D.; Raghavachari, K.; Foresman, J. B.; Cioslowski, J.; Ortiz, J. V.; Stefanov, B. B.; Liu, G.; Liashenko, A.; Piskorz, P.; Komaromi, I.; Gomperts, R.; Martin, R. L.; Fox, D. J.; Keith, T.; Al-Laham, M. A.; Peng, C. Y.; Nanayakkara, A.; Gonzalez, C.; Challacombe, M.; Gill, P. M. W.; Johnson, B. G.; Chen, W.; Wong, M. W.; Andres, J. L.; Head-Gordon, M.; Replogle, E. S.; Pople, J. A. *Gaussian 98*, revision A.6; Gaussian, Inc.: Pittsburgh, PA, 1998.

(56) AMPAC.; 6.55 ed., Semichem Inc.: 7128 Summit, Shawnee, KS 66216, 1999.

(57) In the case of DPB, there is experimental evidence for nonplanarity and/or extensive torsional motion even at low temperatures from the rotationally resolved spectra of DPB recorded by Pratt and co-workers.[113] These workers determined the moments of inertia (I_A^0, I_B^0, I_C^0) of the ground state of DPB to be (202, 3484, and 3675 amu Å^2). The inertial defect,[60] $\Delta^0 \equiv I_C^0 - I_A^0 - I_C^0 = -2 \sum_i m_i r_{iC}^2$, is -10.3 amu Å^2, which implies substantial nonplanarity. These quantities may be compared to values from HF/6-31G(d, p) calculations for the planar geometry (I_A, I_B, I_C, and Δ) = (192, 3484, 3677, and 0 amu Å^2) and for the optimized twisted geometry (194, 3485, 3649, and -30 amu Å^2).

(58) Singh, U.; Kollman, P. *J. Comput. Chem.* **1984**, *5*, 129.

(59) McClellan, A. *Tables of Experimental Dipole Moments*; W. H. Freeman: San Francisco, 1963—1989; Vol. 1—3.

(60) Kroto, H. *Molecular Rotation Spectra*, 2nd ed.; Dover: New York, 1992.

(61) Ely, J.; Haynes, W.; Bain, B. *J. Chem. Thermodynamics* **1989**, *21*, 879.

(62) Allen, M. P.; Tildesley, D. J. *Computer Simulation of Liquids*; Oxford: Oxford, 1987.

(63) These simulations were performed using the program "DL_POLY_2", Smith, W.; Forester, T. R. (CCLRC Daresbury Laboratory, Daresbury, UK, 2001).

(64) Nishikawa, K.; Tanaka, I.; Amemiya, Y. *J. Phys. Chem.* **1996**, *100*, 418.

(65) Frankland, S. J.; Patel, N.; Maroncelli, M., unpublished results.

(66) $g_{ss}(r)$ is normalized relative to a uniform distribution of solvent atoms. This uniform distribution is obtained numerically using a random sampling scheme. The dilute gas limit of $g_{ss}(r)$ comes from an appropriate sampling of the solute solvent pair potential u_{uv}, $g_{ss}^0(r) = \langle \exp\{-u_{uv}/k_BT\} \rangle_r$ as described in ref 10. The "average" depth of the solute—solvent potential can be defined as $\langle u_{uv} \rangle_{min}^{(T)} = -k_BT \ln g_{ss}^0(r_{max})$.

(67) We have also examined the distributions of solvent *molecules* (with positions being defined by the solvent molecule's center of mass) as opposed to solvent *atoms*. The coordination numbers obtained from such distributions are essentially just a factor of 1/3 times the atomic coordination numbers.

(68) Frankland, S. J. V. Solvent Effects on the Raman Spectra of the Isolated C—H Stretches of Cyclohexane-d11: A Molecular Dynamics Study of Liquid and Supercritical Solvation. Ph.D. thesis, The Pennsylvania State University, 1997.

(69) One might expect that hydrogen bonding would be enhanced in the extended conformation of HMS (Figure 1) for steric reasons. Structure #5* of Figure 7 shows that this is not the case. Although structure #5 displays a more classic hydrogen-bonding geometry, the interaction energy is much lower than for #1 due to loss of interactions between the CO_2 and the aromatic system of HMS.

(70) See for example the reviews 10, 8, and 6.

(71) Heidenreich, A.; Bahatt, D.; Ben-Horin, N.; Even, U.; Jortner, J. *J. Chem. Phys.* **1994**, *100*, 6300.

(72) Troxler, T.; Leutwyler, S. *J. Chem. Phys.* **1993**, *99*, 4363.

(73) Dynamical effects on jet-cooled cluster spectra are discussed, for example, in refs 114 and 115. Such effects are not expected to be important in the present cases, which entail large spectral shifts and high temperatures. Furthermore, it is the spectral line shapes, rather than the average frequencies of interest here, which are sensitive to dynamics.

(74) Shalev, E.; Ben-Horin, N.; Even, U.; Jortner, J. *J. Chem. Phys.* **1991**, *95*, 3147.

(75) Information about the $S_0 \leftrightarrow S_1$ transitions in HMS and DPB was obtained from semiempirical AM1/CI calculations using the AMPAC 6.55 program (Semichem Inc., Shawnee KS). Calculations were made for the planar ground-state geometries including between 8 and 12 molecular orbitals in the CI.

(76) Two complicating factors arise in such analyses: (i) the fact that at high densities (i.e., at $2\rho_c$) the frequencies in CO_2 do not perfectly match the liquid—gas correlation and (ii) the fact that ϵ does not adequately represent the polarity of CO_2 for solvatochromic purposes. Both of these complications are discussed at length in ref 9.

(77) It is interesting to note that, because the shifts in both solutes are dominated by the $f(n^2)$ term, and because $f(n^2)$ is approximately proportional to solvent density, approximate $\Delta\rho_{eff}$ values can be read off of the top panels in Figures 9 and 10 as the horizontal difference between the experimental data and the dashed lines.

(78) The densities used to define $\Delta\rho_{eff}^{(N_1)}$ are true densities, i.e., they are simply proportional to numbers of atoms or molecules in a given region of space. In contrast, experimental observables such as UV frequency shifts report on the solute's local environment through some sort of weighted integral over contributions from the entire solvent volume. For observables such as spectral shifts and solvation energies, the weighting is short-ranged (for example as r^{-6} in eq 2 or r^{-4} in eq 5) and therefore most influenced by conditions in the 1st solvation shell, but there is no guarantee that the weighting will provide values directly comparable to 1st shell coordination numbers. Nevertheless, in the present simulations, as well as simulations of other nondipolar systems,[65] it is usually the case that spectral shifts and solvent—solute interaction energies in general closely track the behavior of N_1 as a function of solvent density. For example, the data in Table 2 shows that the quantities U_{LJ}, $\Delta\nu_{\#1}$, and $\Delta\nu_{\#2}$ normalized by N_1 vary by only a few percent over the density range studied. (The total energy and especially the electrical component of the solvation energy do not follow N_1 as closely.) Thus, if any of the quantities U_{LJ}, $\Delta\nu_{\#1}$, or $\Delta\nu_{\#2}$ were used to calculated effective densities in the manner applied to experimental data, they would produce $\Delta\rho_{eff}(\rho)$ curves virtually identical to $\Delta\rho_{eff}^{(N_1)}(\rho)$.

(79) Stone, A. *The Theory of Intermolecular Forces*; Oxford University Press: New York, 1996.

(80) Stratt, R. E.; Adams, J. E. *J. Chem. Phys.* **1993**, *99*, 775.

(81) Schroeder, J.; Troe, J. *Annu. Rev. Phys. Chem.* **1987**, *38*, 163.

(82) Hippler, H.; Schubert, V.; Troe, J. *Ber. Bunsen. Phys. Chem.* **1985**, *89*, 760.

(83) Both of the two relations in eq 10 were used to independently determine values of D and the results averaged. In the case of viscosity, only the Green—Kubo relation (eq 9) was used. Averages were taken over all 9 $\alpha\beta$ pairs in the case of η and over all molecules in the case of D.

(84) Versmold, H. *Mol. Phys.* **1981**, *43*, 383.

(85) Detailed simulations of the rotational dynamics of this same CO_2 model have been performed by J. E. Adams and co-workers (to be published).

(86) Free rotor correlation functions were calculated by simply propagating an ensemble of force-free trajectories from samples of thermally distributed angular velocities.

(87) AM1/CI calculations indicate that the $S_0 \leftrightarrow S_1$ transition moment observed in experiment is within a few degrees of the x inertial axis in both solutes.

(88) Hudson, B. S. Linear Polyene Electronic Structure and Potential Surfaces. In *Excited States*; E. C. L., Ed.; Academic Press: New York, 1982; Vol. 6.

(89) Amirav, A.; Sonnenschein, M.; Jortner, J. *Chem. Phys.* **1986**, *102*, 305.

(90) It is reasonable to expect that the character of the radiating state will differ in CO_2 compared to typical liquid solvents where it is nearly pure 1^1B_u. We have observed that the radiative rate of DPB changes 3-fold in going from alkane to perfluoroalkanes. Because the polarizability of supercritical CO_2 even at $2\rho_c$ is even less than that of perfluoroalkane liquids, we expect large differences in CO_2 compared to most liquid solvents.

(91) Preliminary simulations of a flexible model of DPB do not suggest that the rotation times will be greatly affected by intramolecular torsional freedom, but more study is needed.

(92) Gordon, R. G. *J. Chem. Phys.* **1966**, *44*, 1830.

(93) Keyes, T. *J. Chem. Phys.* **1972**, *57*, 767.

(94) In the limit of zero solvent density the translational velocity correlation function $C_t(t)$ never decays. However, the angular velocity correlation functions of an asymmetric free rotor do decay, although not necessarily to zero. In the present case, $C_{\omega x}(t) \cong 1$ for all relevant times, but $C_{\omega y}(t)$ and $C_{\omega z}(t)$ decay appreciably on the few ps time scale.

(95) Hansen, J. P.; McDonald, I. R. *Theory of Simple Liquids*, 2nd ed.; Academic Press: London, 1986.

(96) We have examined the forces and torques in simulations in which the solute is immobilized. The force autocorrelation functions in these systems are quite similar in appearance to those obtained from inversion of the memory function equations, but their correlation times are uniformly larger than the latter functions. The differences range from about 20% to 50% and are greatest at low densities.

(97) Berne, B. J.; Harp, G. D. *Adv. Chem. Phys.* **1970**, *17*, 63.

(98) Bruehl, M.; Hynes, J. T. *J. Phys. Chem.* **1992**, *96*, 4068.

(99) Blokhin, A. P.; Gelin, M. F. *J. Phys. Chem. B* **1997**, *101*, 236.

(100) Jas, G.; Larson, E.; Johnson, C.; Kuczera, K. *J. Phys. Chem. A* **2000**, *104*, 9841.

(101) Fleming, G. R. *Chemical Applications of Ultrafast Spectroscopy*; Oxford: New York, 1986.

(102) Favro, L. D. *Phys. Rev.* **1960**, *119*, 53.

(103) See, for example, the discussion of the decomposition of the friction on vibrational motion in Ref.[24]

(104) Fernandez-Prini, R. *J. Phys. Chem. B* **2002**, *106*, 3217.

(105) Sciaini, G.; Marceca, E.; Fernandez-Prini, R. **2002**.

(106) This expression differs only slightly from the estimate of free rotor times suggested by Bartoli and Litovitz,[116] which are often used for such purposes. The numerical factor of 0.83 is simply more accurate than their value of $2\pi(41/360) = 0.716$.

(107) This behavior with respect to integral friction can be usefully contrasted with cases in which friction at high frequencies is most important, for example, in vibrational relaxation problems. Here, the effects of local density augmentation appear to be directly observable, as for example in the vibrational relaxation rates in refs 23, 21.

(108) Vesovic, V.; Wakeham, W. A.; Olchowy, G. A.; Sengers, J. V.; Watson, J. T. R. *J. Phys. Chem. Ref. Data* **1990**, *19*, 763.

(109) Liu, H.; Macedo, E. A. *J. Supercrit. Fluids* **1995**, *8*, 310.

(110) Liu, H.; Silva, C.; Macedo, E. *Chem. Eng. Sci.* **1998**, *53*, 2403.

(111) Vesovic, V. On Correlating the Transport Properties of Supercritical Fluids. In *Supercritical Fluids*; Kiran, E., Levelt Sengers, J. M. H., Eds.; Kluwer: Dordrecht, 1994; p 273.

(112) Schroeder, J.; Schwarzer, D.; Troe, J. *Ber. Bunsen. Phys. Chem.* **1990**, *94*, 1249.

(113) Pfanstiel, J.; Champagne, B.; Majewski, W.; Plusquellic, D.; Pratt, D. *Science* **1989**, *245*, 736.

(114) Fried, L. E.; Mukamel, S. *J. Chem. Phys.* **1992**, *96*, 116.

(115) Heidenreich, A.; Jortner, J. *J. Chem. Phys.* **1996**, *105*, 8523.

(116) Bartoli, F.; Litovitz, T. *J. Chem. Phys.* **1972**, *56*, 413.